Climatic and tectonic effects on the origin and evolution of the Dereiçi travertines (the Başkale Basin, Eastern Türkiye), and neotectonic implications

Çetin YEŞİLOVA[1, *]

[1] Yüzüncü Yıl University, Department of Geological Engineering, 65080, Van, Türkiye

Yeşilova, Ç. 2022. Climatic and tectonic effects on the origin and evolution of the Dereiçi travertines (the Başkale Basin, Eastern Türkiye), and neotectonic implications. Geological Quarterly, 66: 27, doi: 10.7306/gq.1659

The Başkale Basin is located in the easternmost part of Türkiye, within a tectonically active area, and located at the intersection of Europe, Asia and the Middle East. In this study, the Dereiçi travertines, one of the most important products of neotectonism in the basin, were investigated sedimentologically, mineralogically and geochemically. To understand the neotectonic evolution of the travertine succession, the sequence was studied from bottom to top as regards morphology, lithofacies and U/Th dates. Crystalline crust, coated gas bubbles, shrub, paper-thin raft and palaeosol lithofacies have been detected in the Dereiçi travertines, which are morphologically of layer type, two ridge types and terrace type. The Dereiçi travertines commenced to precipitate at the intersection of the Işıklı and Ilıcak faults at 255.56 ±9.01 ka, and their deposition continues today. Travertine deposition paused twice between 198.31 ±18–143.07 ±1.5 ka and 96.73 ±8.34–61.59 ±5.4 ka, when palaeosol development took place. According to field and laboratory studies, the Dereiçi travertines developed under climate and tectonic control. The Işıklı and Ilıcak faults played active roles in the development of the travertines. As the travertine ages are linked to movement on both faults, the age of the Işıklı Fault should be 255.56 ±9.01 ka or earlier, and that of the Ilıcak Fault should be 143.07 ±1.5 ka or earlier.

Key words: Başkale Basin, Dereiçi travertines, U/Th dating, lithofacies, palaeoclimate.

INTRODUCTION

The study area is located south-east of Lake Van (eastern Türkiye; Fig. 1A), at the north-west end of the Başkale Basin, whose western and eastern edges are controlled by faults, between the Bitlis Zagros suture zone and the Guilato–Siahcheshmeh–Khoy Fault system in north-west Iran (Sağlam Selçuk and Düzgün, 2017). The basin extends from north-east to south-west, and is 10–15 km wide and 80 km long (Emre et al., 2012; Sağlam Selçuk, 2016; Sağlam Selçuk and Düzgün, 2017). Although many studies focus on the tectonic evolution of the Lake Van basin (Çukur et al., 2013; Koçyiğit, 2013; Toker, 2013, 2014; Sağlam Selçuk, 2016; Toker et al., 2017a, b; Toker and Tur, 2018; Toker and Şahin, 2019), the evolution of the Başkale Basin has been neglected. The Başkale Fault Zone, forming the Başkale Basin, starts from Yavuzlar village in the north-east (Sağlam Selçuk and Düzgün, 2017) and extends to Dereiçi village in the south-west.

The basin and its surroundings include (i) Pre-Neogene rocks consisting mainly of marble and schists, (ii) Neogene volcanic rocks such as basalt, ignimbrite, and (iii) Quaternary deposits including alluvial sediments and travertines (Boray, 1975; Göncüoğlu and Turhan, 1984; Ricou, 1971; Yılmaz, 1971, 1975). Pre-Neogene rocks and Quaternary deposits are exposed clearly in the study area. Paleozoic–Mesozoic metamorphic rocks of the Bitlis Massif form the basement (Fig. 1C). The Bitlis Massif, the largest metamorphic massif in Türkiye, is made up of low- to high-grade metamorphic rocks (Yılmaz, 1975; Tolluoğlu, 1981; Şengün, 1984; Göncüoğlu and Turhan, 1985; Helvacı and Griffin, 1985). The Yüksekova Complex, consisting of Upper Cretaceous granitic and dioritic rocks together with aplitic veins cutting these rocks, unconformably overlies the basement (Perinçek, 1979) and is unconformably overlain by the lower and middle Eocene Durankaya Complex, comprising shale, sandstone, and limestone (Perinçek, 1990). Travertines and recent alluvium developed, related to NE–SW trending strike-slip faults that formed as a result of tectonic movements, and these unconformably overlie the previous units (Yeşilova, 2021; Fig. 1C).

Travertines are formed by the deposition and accumulation of calcium carbonate along a fault line, where groundwater rich in calcium and bicarbonate comes to the surface (Pedley, 1990; Ford and Pedley, 1996; Guo and Riding, 1998; Pentecost, 2005; Gandin and Capezuoli, 2008). Because of these features, travertines are mostly found in geothermal fields (Muir-Wood, 1993; Chafetz and Folk, 1984; Sibson et al., 1975; Altunel and Hancock, 1993a, b; Griffiths and Pedley, 1995; Pentecost, 1995, 2005; Guo and Riding, 1998; Özkul et al., 2002; Piper et al., 2007; Faccenna et al., 2008; Mesci et al., 2008) and follow the fracture system (Altunel and Hancock, 1993b; Guo and Riding, 1998; Fouke et al., 2000; Pentecost, 2005; Veysey et al., 2008; Guido et al., 2010; Guido and Camp-
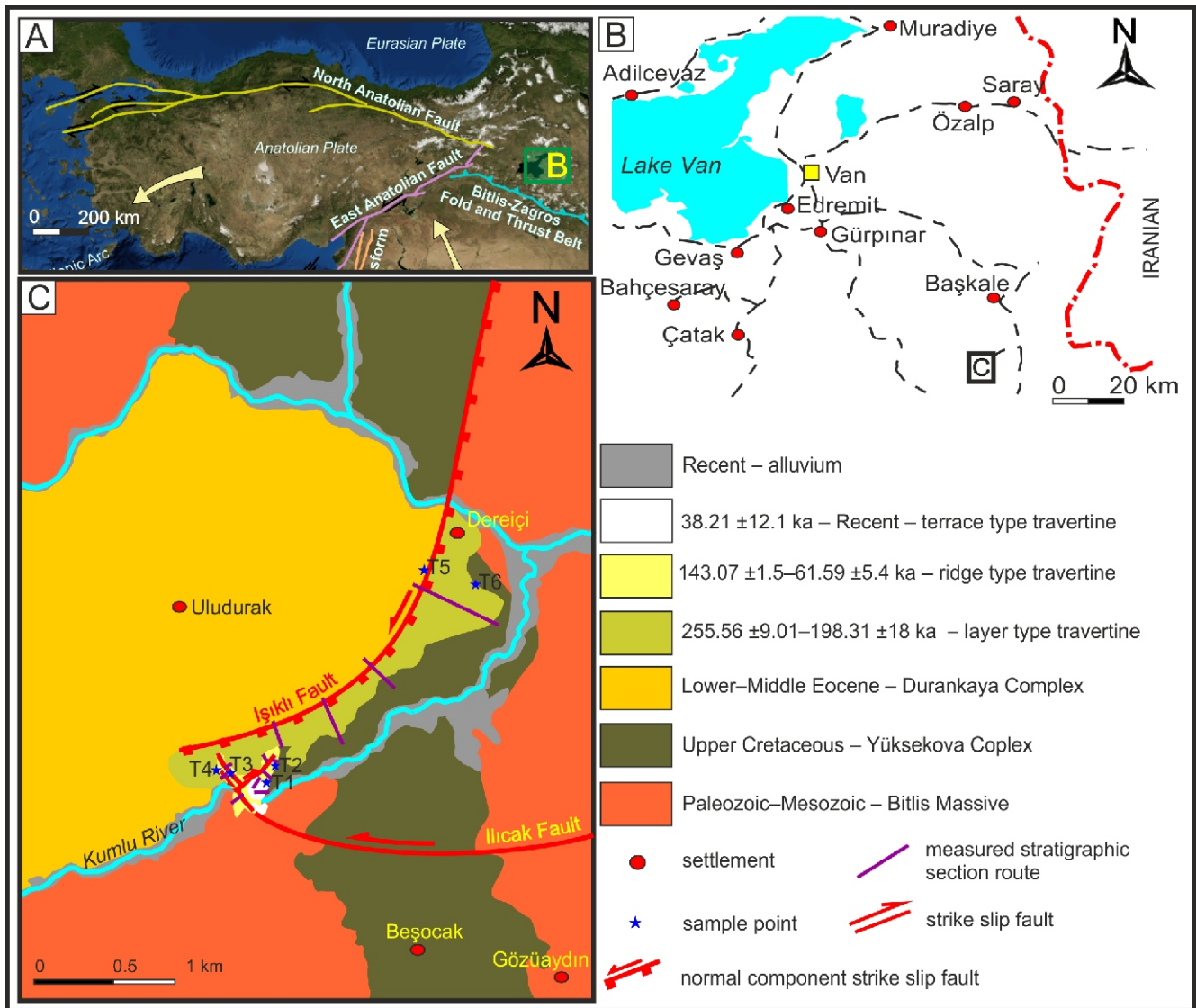
Fig. 1A – location map of the study area, the arrows indicate the direction of movement of the plates; B – map showing the location of the travertines (C); C – geological map of the study area and surrounding region (sample locations are shown with letter T on the map, all faults shown on the map are revised after Sağlam Selçuk and Düzgün (2017)

bell, 2011; Yeşilova et al., 2019, 2021). Many parameters, the most important of which is palaeomorphology, affect the development and morphology of travertines (Ordonez et al., 1986; Pentecost, 1995; Guo and Riding, 1998), such as tectonics (Altunel and Hancock, 1993b; Guo and Riding, 1998; Fouke et al., 2000; Pentecost, 2005; Brogi and Capezzuoli, 2009, 2014) and climate (Pedley, 1990; Andrews, 2006; Toker et al., 2015; Toker, 2017; Tagliasacchi-Toker and Kayseri-Özer, 2020; Kandemir et al., 2021). However, many factors control travertine occurrence, including the shape of the source, the chemistry (including calcium content) of the water, morphology, biological activity, and volcanism (Julia, 1983; Barnes et al., 1978; Chafetz and Folk, 1984; Pedley, 1990; Altunel and Hancock, 1993a, b; Ford and Pedley, 1996; Guo and Riding, 1998; Pentecost, 2005; D'Alessandro et al., 2007; Huybers and Langmuir, 2009; Guido et al., 2010; Capezuoli et al., 2014). Palaeosols record the physical, biological, and chemical history of travertine-forming systems (Tabor and Meyers, 2015). The name of palaeosol is given to ancient soils formed due to the interaction of the lithosphere, hydrosphere, biosphere and atmosphere

(Kraus, 1999; Retallack, 2014; Tabor and Meyers, 2015). Palaeosols are frequently used in palaeoclimate assessments due to their high pollen content (e.g., Richmond, 1962; Bertini et al., 2014; Tagliasacchi-Toker, 2018; Tagliasacchi-Toker and Kayseri-Özer, 2020), and their presence also indicates that weathering processes began and thus travertine occurrence ceased (Chafetz and Folk, 1984; Guo and Riding, 1998; Özkul et al., 2002; Van Noten et al., 2018). Palaeosol occurrence can also occur with a change in direction of the thermal waters that make up the travertine (Brogi et al., 2012; Capezzuoli et al., 2014; Gandin and Capezzuoli, 2014; Brogi et al., 2016).

This study determines the deposition and development of the Dereiçi travertines in the Başkale Basin, notably the effects of climate, tectonism, magmatism, biological activity and groundwater on this travertine deposit. These help constrain the parameters controlling the age and development of Dereiçi travertines. This study is the first to detail the occurrence of travertines in the Başkale Basin, a tectonically active area on the Eastern Anatolian Plateau, and also contributes to understanding the tectonic evolution and climate dynamics of the area.

MATERIALS AND METHODS

The study area covers an average area of 20 km^2 between the villages of Dereiçi, Uludurak and Beşocak. In this area, measured stratigraphic sections were made of each travertine succession detected, and travertine lithofacies descriptions/interpretations were made. Sections were measured at the best travertine exposures, of which four sections were of layer type, three of a first ridge type, three of a second ridge type and two were of terrace type travertines (Fig. 1C). The generalized columnar section was derived by correlation of related successions (Fig. 2).

For U/Th radiometric analysis, samples were obtained from the lower and upper parts of each succession. In addition, for petrographic analysis involving thin section petrography, scanning electron microscopy and energy dispersive X-ray spectroscopy (SEM-EDX), 52 samples were selected from the travertine successions. Petrographic thin sections were made from 40 samples, and SEM-EDAX analysis was performed on 12 samples. Six samples, from the lower and the upper parts of each travertine succession, were sent for U/Th age dating. The UTM coordinates for the corner points of the study area and for the samples taken for U/Th analysis are given in Table 1.

Field study. In the field studies, each travertine unit was identified separately, and the stratigraphical relationship of the travertines was determined and related to the regional tectonic history. The succession, which is locally obscured by overburden, was established by tracing lateral continuity. Four travertine morphologies were identified in this study. These are (i) layer type travertines, (ii) first ridge type travertines, (iii) second ridge type travertines and (iv) terrace type travertines. Lithofacies and lithofacies associations were determined according to their lithological characteristics (layer location, layer thickness, colour, macrofossil content, macrotexture, porosity, etc.; e.g., Julia, 1983; Chafetz and Folk, 1984; Pedley, 1990; Ford and Pedley, 1996; Guo and Riding, 1998; Pentecost, 2005; Gandin and Capezuoli, 2008; Capezuoli et al., 2104). Palaeosols in the study area consist of beige-brown and uncon-

solidated sandy-silty and clayey units (e.g., Kraus, 1999; Retallack, 2014; Tabor and Meyers, 2015). Two palaeosol levels were identified in the travertines, which occur both between bedded travertines and ridge travertines, and between two ridge type travertines (Fig. 2).

Defining the faults in the study area was helped by data from previous studies, with factors such as the movement mechanisms and directions being taken into account (Emre et al., 2012; Koçyiğit, 2013; Sağlam Selçuk, 2016; Sağlam Selçuk and Düzgün, 2017). The Işıklı Fault (defined in the study area) is ~5 km away from Işıklı village, causing both lateral (sinistral) and vertical (along-slope) movements within the geological units. As regards its location and kinematic characteristics, the Işıklı Fault recognized in the study area is a continuation of the Işıklı Fault described in previous studies (Sağlam Selçuk, 2016; Sağlam Selçuk and Düzgün, 2017). The layer type travertines were developed on the block moving downslope due to the effect of this fault (Fig. 1C). The Ilıcak Fault was located at an average distance of 7 km from the area where it was originally defined and mapped and along the same direction. Sinistral movement was detected in the units affected by this fault, on which the 1st ridge type travertines were formed (Fig. 1C). The fault lines identified in this study were not excavated, and so more detailed data cannot be provided. Fault definitions were made based on previous studies (Emre et al., 2012; Koçyiğit, 2013; Sağlam Selçuk, 2016; Sağlam Selçuk and Düzgün, 2017) and on movements in the geological units affected.

U/Th analysis. Six samples were collected from lower and upper parts of each travertine occurrence (Fig. 2) and analysed (Table 2). About 40–80 g of sample was prepared by crushing with a hammer. U/Th analyses were performed using a multi-collector inductively coupled plasma mass spectrometer (MC-ICP-MS), Thermo Electron Neptune, in the High-precision Mass Spectrometry and Environment Change Laboratory (HISPEC), Department of Geosciences, National Taiwan University. A triple-spike ^{229}Th-^{233}U-^{236}U isotope dilution method (Shen et al., 2003) was used to correct for instrumental fractionation and to determine U/Th isotopic and concentration (Shen et al., 2012). The half-lives of U-Th nuclides used are available in Cheng et al. (2013). Uncertainties in the U-Th isotopic data and ^{230}Th dates were calculated at the 2s level or two standard deviations of the mean (2s$_m$) unless otherwise stated.

Minerology-Petrography. 52 samples were collected for mineralogical and petrographic analysis: 40 samples for thin sections and 12 samples for SEM analysis.

Thin sections were prepared in the laboratory of Dokuz Eylül University, Torbalı Vocational High School. Oriented matchbox-sized samples were cut and glued to 2 mm-thick frosted glass slides with araldite and hardener. The adhered samples were thinned on an abrasive disc to prepare for examination under the microscope. Mineralogical and petrographic determinations were made according to standard carbonate and established travertine classifications (Folk, 1962; Dunham, 1962; Pentecost, 2005; Riding, 2008).

The SEM samples were examined at the Scientific Research and Application Center of Van Yüzüncü Yıl University, using a type of electron microscope that obtains images by scanning the sample surface with a focused electron beam, providing information about the topography and composition of the sample surface. Both natural and polished sections were coated with Au-Pd for 90 seconds for SEM analysis, and photographed with an SE2 detector.

T a b l e   1

UTM coordinate of study area and sample locations (for U/Th)

UTM coordinate of Study area (38 S)	
Corner point	UTM coordinate
1	408069 E / 4190194 K
2	409712 E / 4189451 K
3	408212 E / 4189444 K
4	406794 E / 4188170 K
UTM coordinate of samples (38 S)	
Sample no	UTM coordinate
T6	409092 E / 4188922 K
T5	408610 E / 4189349 K
T4	407544 E / 4188219 K
T3	407695 E / 4188310 K
T2	407635 E / 4188269 K
T1	407677 E / 4188227 K
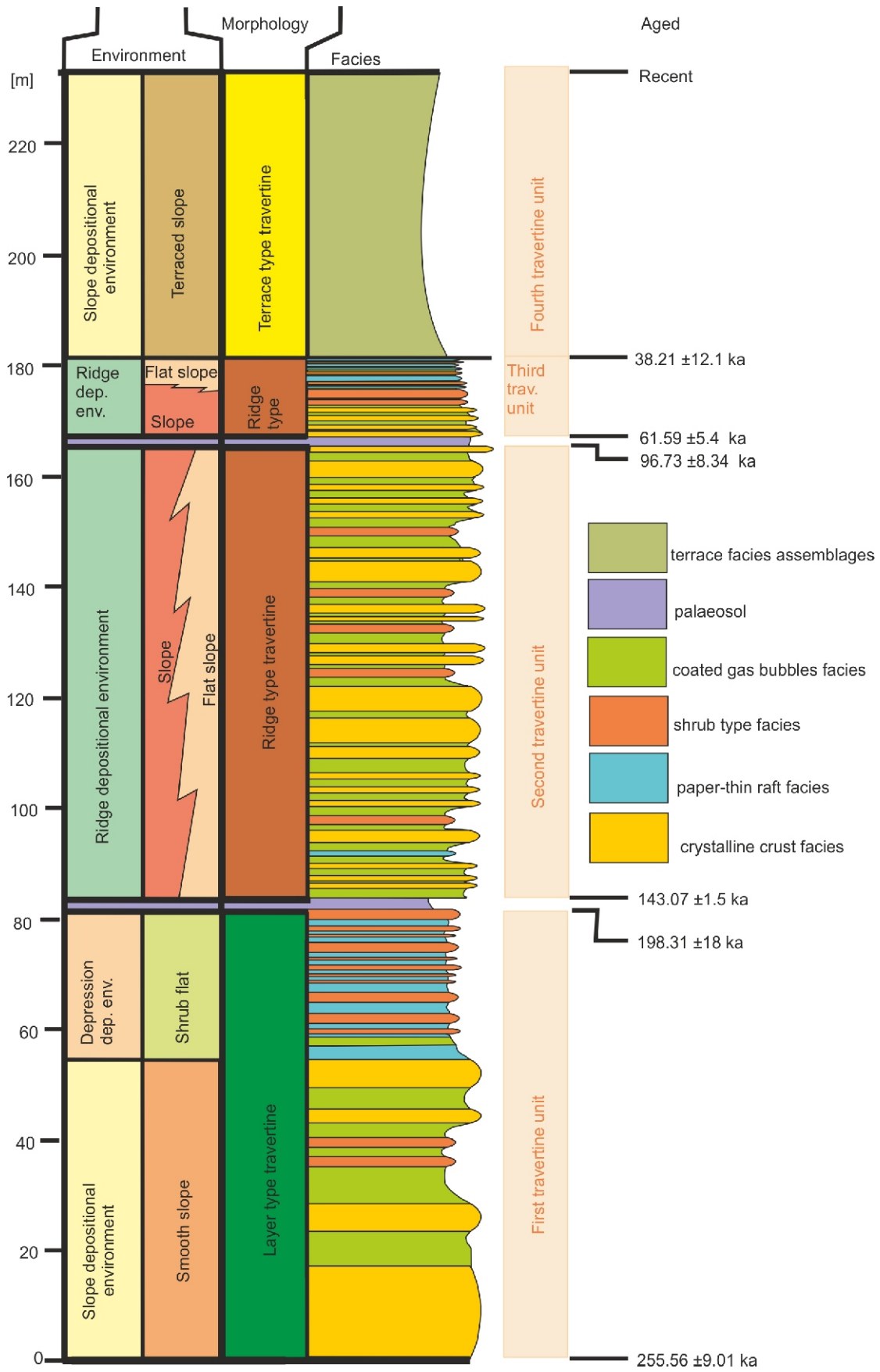
Fig. 2. Stratigraphic section showing the travertine in Dereiçi region

In the cross-section, lithofacies associations and sample locations are indicated

T a b l e 2

Composition of the uranium and thorium isotopes and 230Th ages for the travertine and tufa samples

Sample ID	Weight [g]	238U [ppbᵃ]	232Th [ppb]	234U measuredᵃ	230Th/238U activityᶜ	230Th/232Th atomic (10⁻⁶)	Age (ka ago) uncorrected	Age (ka BP) corrected ᶜ,ᵈ	234U_initial correctedᵇ
T1	0.0814	5406 ±12.85	3987.2 ±211	305.2 ±4.2	0.556 ±0.03	12.43 ±1.00	59.371 ±4.4	38.21 ±12.1	332.34 ±9.9
T2	0.0703	1833 ±2.77	792.2 ±25	181.5 ±1.8	0.556 ±0.02	21.19 ±1.03	69.667 ±3.7	61.59 ±5.4	222.77 ±4.6
T3	0.0940	1807.8 ±3.2	879.1 ±23	255.5 ±3.43	0.8429 ±0.027	28.578 ±1.19	109.55 ±5.4	96.73 ±8.34	320.821 ±7.6
T4	0.0683	3738 ±8.13	21.7 ±0	307.9 ±4.2	1.046 ±0.01	2974.30 ±20.43	143.299 ±1.5	143.07 ±1.5	423.23 ±6.0
T5	0.0560	19.210 ±0.087	13133 ±40	223.6 ±8.4	1.096 ±0.032	26.43 ±0.77	212.069 ±18	198.31 ±18	391.26 ±26
T6	0.0622	26.8 ±0.1	1022 ±7	195.3 ±5.35	1.0761 ±0.007	465.18 ±3.89	256.18 ±9.1	255.56 ±9.01	431.439 ±17.4

Analytical errors are 2 of the mean. ᵃ[²³⁸U] = [²³⁵U] 137.818 (±0.65‰) (Hiess et al., 2012); ᵇ ²³⁴U_Initial corrected was calculated based on ²³⁰Th age (T), i.e., ²³⁴U_Initial = ²³⁴U_measured Xe^I234*T, and T is corrected age. ᶜ$r^{230}Th/^{238}U_{activity} = 1 - e^{-I230T}$ + (²³⁴U_measured/1000)I_I230/(I_I230 − I_234)](1 − e^{-(I230 − I234)T}), where T is the age. Decay constants are 9.1705 10⁻⁶ yr⁻¹ for ²³⁰Th, 2.8221 10⁻⁶ yr⁻¹ for ²³⁴U (Cheng et al., 2013), and 1.55125 10⁻¹⁰ yr⁻¹ for ²³⁸U (Jaffey et al., 1971). ᵈAge corrections, relative to 1950 AD, were calculated using an estimated atomic ²³⁰Th/²³²Th ratio of 4 (±2) 10⁻⁶ . Those are the values for a material at secular equilibrium, with the crustal ²³²Th/²³⁸U value of 3.8. The errors are arbitrarily assumed to be 50%

RESULTS

A generalized travertine stratigraphic column for the area was prepared, taking into account lateral and vertical lithofacies variations (Fig. 2). The Dereiçi travertines, with a total thickness of 232 m and containing four different travertine successions, consist of 5 different lithofacies (Fig. 2). The travertines occur at the intersection points of the Işıklı dextral strike-slip fault with a normal component and NNE–SSW trend and the Ilıcak left-lateral strike-slip fault of NE–SW trend (see Fig. 1C).

At the base of the sequence are layer type travertines formed between 255.58 ka and 198.31 ±18 ka (255.56 ±9.01–198.31 ±18 ka at the base of the first travertine unit; Fig. 3A, B). Ridge type travertines above the layer type travertines were formed between 143.07 ±1.5–96.73 ±8.34 ka (second travertine unit). The overlying second ridge type travertines formed at about 61.59 ±5.4 ka (third travertine unit). Lastly, from 38.21 ±12.1 ka, terrace type travertines (fourth travertine unit) formed on the southeastern slope of the second ridge type travertines (Fig. 3G). Terrace-type travertines still continue to form (see Figs. 1C and 2).

MORPHOLOGICAL CLASSIFICATION

Layer type travertine. This is observed in the field as cream-yellow, medium to thick bedded travertine. Its morphology consists of 4 different travertine lithofacies including crystalline crust, shrub, coated gas bubbles and paper-thin raft lithofacies. Travertines in the first 55 metres of the 81-metre thickness include an alternation of crystalline crust, shrub and coated gas bubble lithofacies (Fig. 2). In the remaining 26 metres of this type, there is an alternation of shrub and paper-thin raft lithofacies (Fig. 2). This travertine developed along the last 2 kilometres of the southern tip of the Işıklı Fault (see Fig. 1C).

First ridge type travertine. These travertines, which overlie the layer type travertines, are 85 metres thick, being separated from them by a 2 metre-thick palaeosol (Fig. 2). This light to dark brown travertine formed along the Ilıcak left-lateral strike-slip fault at its intersection with the Işıklı normal component-left-lateral strike-slip fault. Its length is ~500 m (Fig. 3C, D). Crystalline crust and coated gas bubbles lithofacies form the main lithofacies, accompanied by shrub lithofacies. Only one instance of paper-thin raft lithofacies was observed in the section. There is locally a waterfall lithofacies association on the steep slopes of this travertine type (Fig. 3D).

Second ridge type travertine. This starts with a palaeosol level at the base, as with the first ridge type travertine (Fig. 2). This travertine morphology, with a total thickness of 13 metres, has four different lithofacies: crystalline crust, shrub, coated gas bubbles and paper-thin raft (Figs. 2 and 3E, F). This morphology was formed by waters carried upwards due to a fracture that opened on the north-east slope of the first ridge type travertine (see Fig. 1). Terrace type travertines formed on the southeast slopes of the NE–SW trending travertines. An alternation of crystalline crust and coated gas bubbles lithofacies was found in the lower parts of the travertine succession, and an alternation of shrub and paper-thin raft lithofacies in the upper parts (Fig. 2).
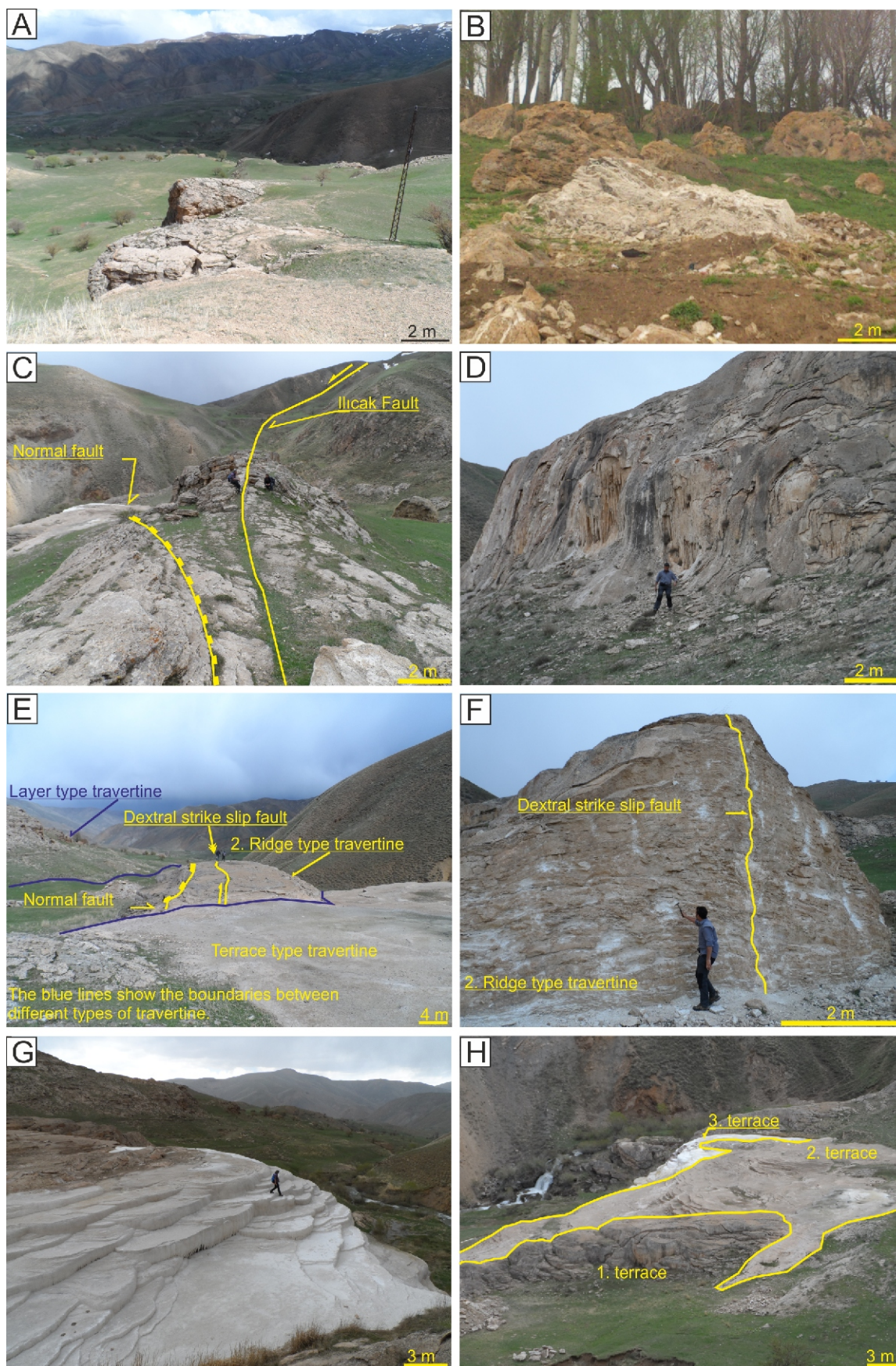
Fig. 3. Different travertine units in the study area

A, B – terrace type travertine, **C–F** – ridge type travertine, **G, H** – terrace type travertine

Terrace type travertine. This travertine unit formed in three different periods; first, second and third. The travertines completely dried and ran out of water in the first period. These travertines are a common weathering product, and were affected by tectonism (Fig. 3H). In the second period, semi-current travertines formed, the lower parts of which represent completely dry conditions, while the upper parts have water outlets in places. Weathering processes have also started in these travertines (Fig. 3H). Current travertines ranging in colour from white to cream are situated at the south end of the terrace type travertines (Fig. 3G, H). The terrace type travertines become younger as the distance from the crack axis of the second ridge type travertine increases (i.e. they become younger towards the south-east). The total thickness of the travertine succession reaches ~56 m.

TRAVERTINE LITHOFACIES

Within the travertine succession, 5 different lithofacies types were distinguished: crystalline crust, shrub, coated gas bubbles, paper-thin raft and palaeosol (Figs. 2 and 3). Crystalline crust and coated gas bubbles lithofacies are the most frequent types in the field. Lithofacies definitions and naming are based on previous studies (Chafetz and Folk, 1984; Guo, 1993; Guo and Riding, 1998; Ozkul et al., 2002; Gandin and Capezzuoli, 2008; Capezzuoli et al., 2014).

Crystalline crust lithofacies. The deposits of this lithofacies are cream-beige in colour, and have a slightly porous structure (Figs. 2 and 4A). Thicknesses of layers vary from 0.6 to 45 cm.

Coated gas bubbles lithofacies. This is one of the most common lithofacies in the field, being repeated 30 times or more in the entire travertine succession (Fig. 2). The layers, 0.3 to 45 cm thick, have beige and white colours and are highly porous (Fig. 4B).

Shrub lithofacies. The layers of this lithofacies are beige-white, and alternate with layers of paper-thin raft lithofacies. Their thickness ranges from 1 and 20 cm (Fig. 2). This lithofacies shows three different forms in the field: (i) as longitudinally growing shrubs between aragonite layers, (ii) as dwarf shrubs within layers, and (iii) as tiny shrub balls in terrace pools (Fig. 4C, D).

Paper-thin raft lithofacies. The layers of this lithofacies are the least frequent, and alternate with layers of shrub lithofacies in their upper parts. They were observed in the upper parts of the layer type and second ridge type travertines in the study area (Fig. 2). The thickness of the beige and brown layers ranges from 0.7 and 5 cm (Fig. 4E).

Palaeosol. Palaeosols, beige-brown in colour, are present at different levels of the sequence, and are calcareous in their upper parts due to alteration of the overlying travertine (Figs. 2 and 4H). The thicknesses of the lower and upper palaeosol levels are ~2 m and 1.5 m, respectively (Fig. 4H). These thicknesses decrease further down the slope. While the palaeosols examined in the Dereiçi region overlie an irregular travertine surface, sharply defined travertines rest on top of them.

MINERALOGY AND PETROGRAPHY

The calcite of the crystalline crustal lithofacies IS mostly observed as limpid calcite crystals (sparry; Fig. 5A–C, E); there are very few micritic occurences (Fig. 5L, P, Q), While calcite crystals developed as individual crystals perpendicular to the growth axis (Fig. 5B, C, E) are observed occasionally (Fig. 5A).

In places the upper surfaces of bundles of crystals exhibit sinuous textures, while elsewhere they consist of conchoidal fans (Fig. 5A–C, E). Calcite growth lines have a sinuous texture within thin calcite laminae (Fig. 5A–C, E). Calcite crystals forming crystal fans display conspicuous extinction under cross-polarized light (Fig. 5A–C). The calcite laminae vary in thickness. There are also occasional Si- and Mg-bearing nodules of in the bundles of calcite crystals (Fig. 5C–D). Si, Fe and Mn together with irregular calcite crystals were identified in the paper-thin raft lithofacies (Fig. 5F, G). Microbial mats and minerals occur together in the raft-type lithofacies (Fig. 5F, O). These microbial mats developed around the minerals (Fig. 5F, O). Shrubs, with superimposed leaves, resemble thin fans growing along their long axis (Fig. 5H, I), like the leaves of a short shrub (Fig. 5I), and these shrubs are surrounded by microbial mats (Fig. 5J). Again, as for all other lithofacies, Si-bearing grains are encountered in this lithofacies (Fig. 5J, K). The crystalline crustal lithofacies involves intercalations of aragonite crystals and rods (see Figs. 4C, F and 5M). These aragonite rods are placed in superposition and perpendicular to the bedding planes (see Figs. 4C and 5M).

INTERPRETATION OF FACIES ASSEMBLAGES

Lithofacies types can be used to interpret many aspects such as distance from source, depositional environment, pauses in travertine deposition, and fault/fracture activity (Kitano, 1963; Chafetz and Folk, 1984; Folk et al., 1985; Chafetz et al., 1991; Ford and Pedley, 1996; Guo and Ridding, 1998; Özkul et al., 2002). Therefore, each lithofacies can represent a different environment.

These travertines indicate different environmental conditions during growth of the lithofacies forming the travertines (e.g., biological activity, mineralogical and petrographic characteristics, water regime, dip, occurrence temperature) and different lithotypes. These environmental conditions produce different lithofacies associations (Guo and Riding, 1998; Özkul et al., 2014). The travertines are classified into three main lithofacies associations and four sub-lithofacies associations using the nomenclature of Guo and Riding (1998). Major lithofacies associations include slope, ridge and depression depositional environments. When reconstructing the depositional environments, parameters such as the temperature of the water, the slope of the layers, morphology, location of the main fracture, layer thicknesses, horizontality of the layers forming the facies, cement type (micrite/sparite) and biological activity are taken into account (e.g., Guo and Riding, 1998; Özkul et al., 2014; Capezzuoli et al., 2014).

SLOPE DEPOSITIONAL ENVIRONMENT

This lithofacies association is represented by two sub-lithofacies associations in the field area, consisting of smooth slope lithofacies assemblages and terraced slope lithofacies assemblages. Smooth slope lithofacies assemblages are morphologically composed of layer type travertines (see Fig. 2). This sub-lithofacies association also forms the base of the slope depositional environment lithofacies assemblage. Terraced slope lithofacies assemblages are morphologically composed of terrace type travertines (see Fig. 2). This sub-lithofacies association forms in the top of slope depositional environment lithofacies assemblage.

Smooth slope lithofacies assemblages. This lithofacies association is represented by crystalline crust, coated gas bub-
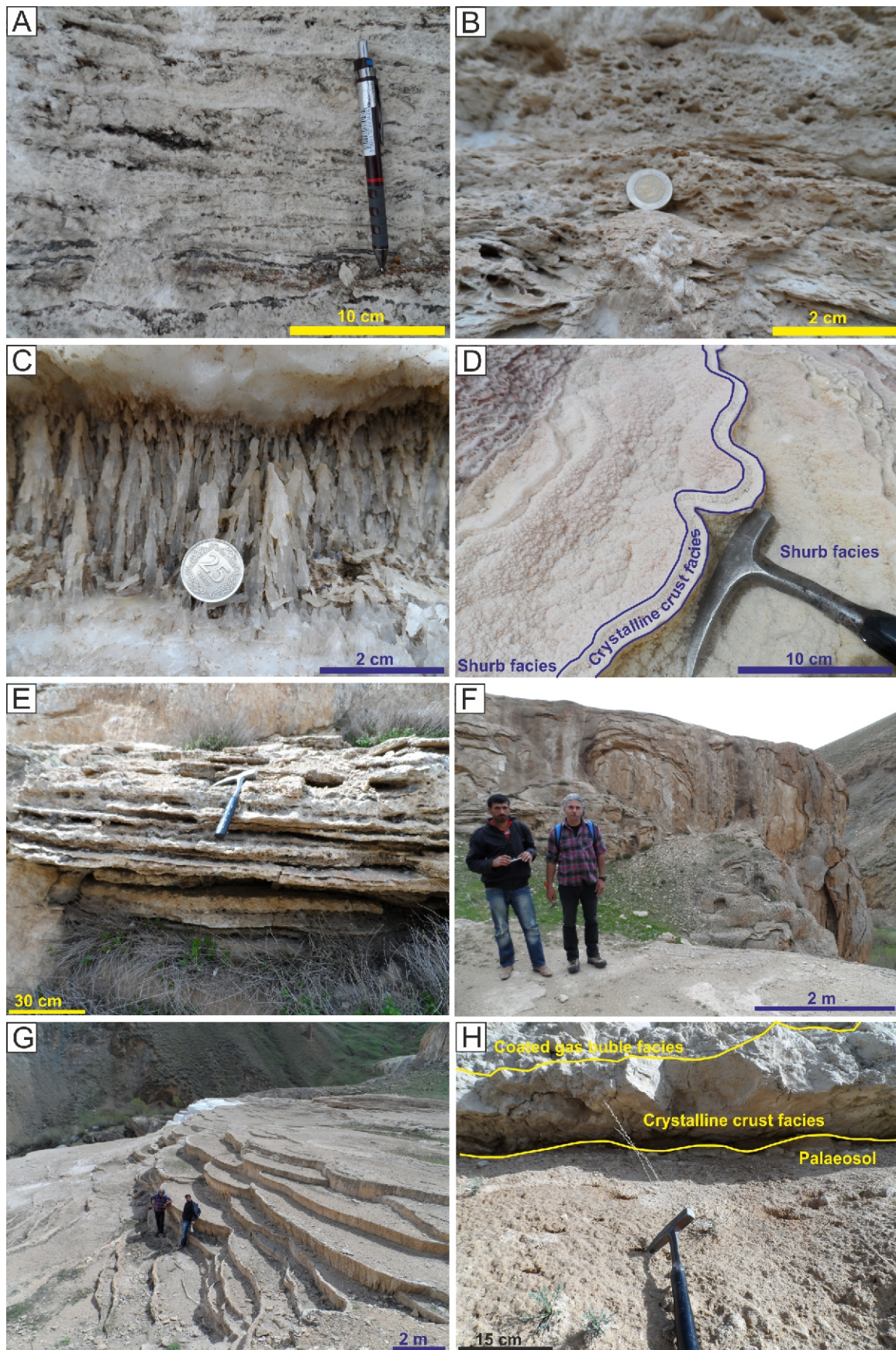
Fig. 4. Different lithofacies types forming the travertines

A – crystalline crust lithofacies; **B** – coated gas bubbles lithofacies; **C**, **D** – shrub lithofacies; **E** – paper-thin raft lithofacies; **F** – waterfall lithofacies association; **G** – terrace lithofacies assemblages; **H** – palaeosol, crystalline crust, coated gas bubbles lithofacies
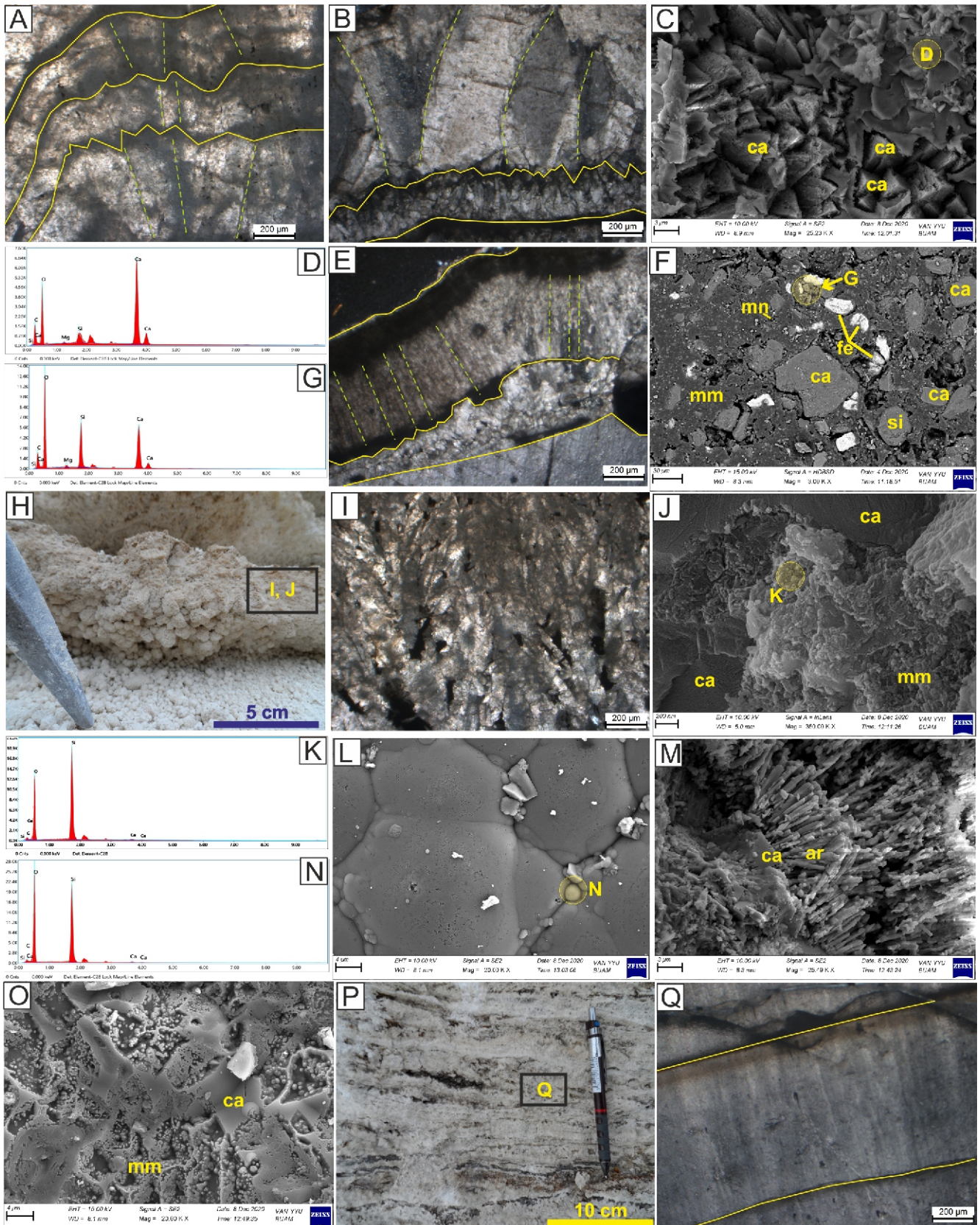
Fig. 5. Thin section, SEM and EDX images of travertine lithofacies

A, B, E, I, Q – thin section images of lithofacies; note that the calcite fans in (a and e) are not of equal thickness; shrub (**C, F, J, L, M, O**) SEM images of lithofacies; **H** – shrub lithofacies; **D, G, K, N** – EDX analysis of SEM images; **P** – crystalline crust lithofacies; ca – calcite, mm – microbial mat, ar – aragonite, si – silicon, fe – iron, mn – manganese

ble and shrub lithofacies with a total thickness of 55 metres. The crystalline crust lithofacies is 33 metres, the coated gas bubbles lithofacies is 19 metres, and the shrub lithofacies is 3 metres thick (see Fig. 2). The dip angle of the slope depositional environment varies between 25 and 35°. The crystalline crust lithofacies mainly occurs in source areas where water temperature and energy are high (e.g., Guo and Riding, 1998). The coated gas bubbles lithofacies formed from hydrothermal fluids with high gas content (Özkul et al., 2014). Considering these features of the lithofacies, this lithofacies association occurs in warm water slope environments where rapid water flow and less biological activity are observed (e.g., Guo and Riding, 1998). The sinuous texture of calcite growth lines, with an upwards trend in thin calcite laminae, indicates that these crystals grew perpendicular to the depositional axis (Özkul et al., 2001). That the calcite crystals examined are perpendicular to the bedding planes and have a thin structure indicates limited biological activity and thus rapid water flow. Because the flow rate of the water forming the calcite crystal fans was not constant, these crystal fans developed with different sizes (see Fig. 6A, B, E) (e.g., Özkul et al., 2001; Jones, 2017; Luo et al., 2021).

Terraced slope lithofacies assemblages. This is the last lithofacies association, with a thickness of 46 m at the top of the sequence. Travertine terrace pools are represented by the shrub lithofacies and waterfall lithofacies association growing in pools. The edges of these pools are composed of crystalline crust lithofacies, while the terrace pools are made up of paper-thin raft, shrub and coated gas bubble lithofacies. The waterfall lithofacies association is beige-white, observed in the study area on the walls of the pools of the terrace type travertines and on the wall of the first ridge type travertines (Figs. 3D, G and 4F, G). On the edges of the terrace pools, the lithofacies association is 10–80 cm-thick and beige-white, while on the walls of the first ridge type travertine it is 10–15 cm-thick and brown (Figs. 3D, G and 4 F, G). The uppermost levels of the first ridge type lithofacies association are formed by the crystalline crust lithofacies. However, the uppermost crystalline crust lithofacies laterally transitions into the waterfall lithofacies association. Therefore, the waterfall lithofacies association is not shown on the first ridge type travertines in the section. Likewise, since all lithofacies found in terrace type travertines were examined in terrace lithofacies assemblages, this lithofacies association was not shown in the section (see Fig. 2). This lithofacies association still continues to form. The temperature of the waters varies presently from 12 to 17°C, mostly due to seasonal temperature changes. The average air temperature difference between summer and winter is ~40°C. The growth of the shrubs in the terrace pools and the microbial mats in the SEM images indicates organic activity (see Fig. 5H–J). The waterfall lithofacies association is surrounded and covered by shrub lithofacies (e.g., Guo and Riding, 1998). The location and landscape of deposits and lithofacies characteristics show that this lithofacies association developed in the form of terraces overflowing with water, the terrace walls formed by the overflowing water on steep slopes (e.g., Chafetz and Folk, 1984; Guo and Riding, 1998).

RIDGE DEPOSITIONAL ENVIRONMENT

This lithofacies association is represented by slope and flat slope lithofacies assemblages with sub-lithofacies associations.

Slope lithofacies assemblages. The crystalline crust lithofacies includes an alternation of coated gas bubbles and shrub lithofacies, just like the smooth slope lithofacies assemblages. These assemblages have similar features to the smooth slope lithofacies as regards mineralogical and petrographical components. The main difference between the two lithofacies associations is that smooth slope lithofacies assemblages formed by water flowing down the slope in front of the fault (layer type travertine). However, slope lithofacies assemblages were formed in ridge type travertines. This lithofacies association formed as a result of a vertical fault on a 30° slope, with regular water flow along the fault (e.g., Guo and Riding, 1998; Özkul et al., 2014). The lithofacies association formed in ridge deposition environments may be described with reference to both plant content and petrographic characteristics (e.g., Guo and Riding, 1998; Özkul et al., 2014).

Flat slope lithofacies assemblages. Environments where the slope angle starts to decrease are termed flat slope (Özkul et al., 2014). In the first ridge type travertines, it is represented by crystalline crust and shrub type lithofacies, while in the second ridge type of travertines, it consists of shrub and paper thin-raft lithofacies. In the field, these are found in lateral continuity with the slope lithofacies assemblages (first ridge type travertine) or on slope lithofacies assemblages whose layer slopes are close to horizontal (second ridge type travertine) (see Fig. 2). Layer thicknesses vary between 3 and 8 cm. Thin layers indicate that the water flow slowed down on the flattened topography (e.g., Guo and Riding, 1998; Özkul et al., 2014). While the waters emerging from the fracture on the slope form the slope lithofacies assemblages on both sides of the fault, the flat slope lithofacies assemblages are formed with slope lithofacies assemblages in areas where the slope becomes flatter (e.g., Guo and Riding, 1998; Özkul et al., 2014).

DEPRESSION DEPOSITIONAL ENVIRONMENT

This lithofacies association is represented by the sub-lithofacies association of shrub flat lithofacies assemblages.

Shrub flat lithofacies assemblages. Shrub flat lithofacies assemblages were first used by Guo (1993) and Guo and Riding (1998). The main characteristics of this lithofacies association are horizontal, near-horizontal light-coloured and thin-bedded layers, spreading laterally over large areas. However, in this study, paper-thin raft lithofacies with the same features will be included in this sub-lithofacies association. The shrub-like short plants, microbial activity, and travertine rafts indicate that the environment was a bush plain and on occasion it changed to a lacustrine environment (Chafetz and Folk, 1984; Guo and Riding, 1998; Özkul et al., 2014; Capezzuoli et al., 2104; Kandemir et al., 2021). It is understood that this sub-lithofacies formed within the depressional depositional environment, considering the environmental parameters of both lithofacies described above (e.g., Guo and Riding, 1998; Özkul et al., 2014).

DISCUSSION

FACTORS CONTROLLING THE OCCURRENCE OF TRAVERTINE

Many factors control the occurrence of travertine, such as calcium content, biological activity, morphology, shape of source, amount of water, climate, tectonism and magmatism (Julia, 1983; Barnes et al., 1978; Chafetz and Folk, 1984; Pedley, 1990; Altunel and Hancock, 1993a, b; Ford and Pedley, 1996; Guo and Riding, 1998; Pentecost, 2005; D'Alessandro et al., 2007; Huybers and Langmuir, 2009; Guido et al., 2010; Capezuoli et al., 2104; Yeşilova et al., 2021). Here, climate (Lisiecki and Raymo 2005; North Greenland Ice Core Project members, 2004; Steffensen et al., 2008; Svensson et al., 2008; Wolff et al., 2010; Barker et al., 2011; Litt et al., 2014; Toker et
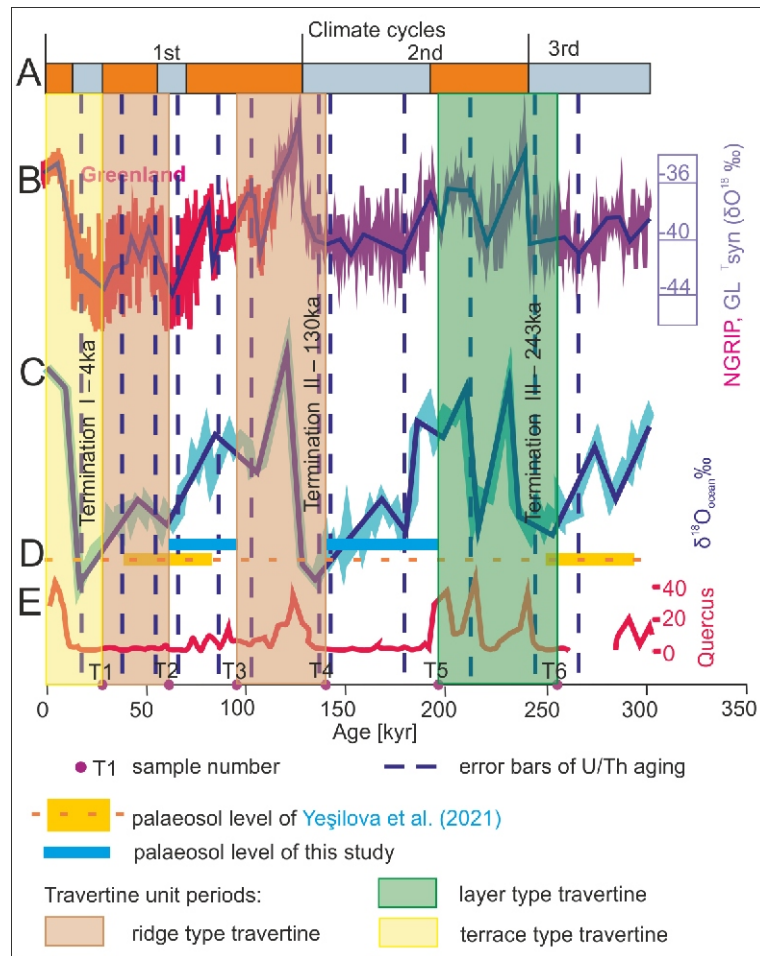
Fig. 6. Comparison of Dereiçi travertine succession with marine core-ice core stratigraphy by Lisiecki and Raymo (2005)

A – includes 3 glacial-interglacial periods, respectively; **B** – NGRIP/GLT-syn and ^{18}O values (North Greenland Ice Core Project members, 2004; Steffensen et al., 2008; Svensson et al., 2008; Wolff et al., 2010; Barker et al., 2011); **C** – Marine Isotope Stage (MIS) (stack of 57 globally distributed benthic ^{18}O records; **D** – simultaneously, the comparison of this study with Yeşilova et al. (2021), blue boxes indicate palaeosol occurrence times, yellow boxes indicate the palaeosol levels in Yeşilova et al. (2021); **E** – Lake Van *Quercus* pollen by Litt et al. (2014)

al., 2015), tectonism (Koçyiğit, 2013; Emre et al., 2012; Sağlam Selçuk, 2016; Sağlam Selçuk and Düzgün, 2017; Kandemir et al., 2021), magmatism (Keskin, 2003; Özdemir et al., 2006; Lebedev et al., 2010; Özdemir and Güleç, 2014; Oyan et al., 2016, 2017; Oyan, 2018a, b; Açlan and Altun, 2018), source area and geomorphology are discussed in detail.

Four different stages are represented in the Dereiçi travertines (Fig. 2). They can be ordered as follows: (i) layer type travertine between 255.56 ±9.01 ka and 198.31 ±18 ka, (ii) ridge type travertine between 143.07 ±1.5 ka and 96.73 ±8.34 ka, (iii) ridge type travertine between 61.59 ±5.4 ka and 38.21 ±12.1 ka, and (iv) terrace type travertine between 31.21 ka to recent times. The formation of travertines evidently paused twice at the palaeosol levels due to weathering and erosion processes. The first pause occurred between 198.31 ±18 and 143.07 ±1.5 ka and the second one occurred between 96.73 ±8.34 and 61.59 ±5.4 ka (e.g., Kraus, 1999; Retallack, 2014; Tabor and Meyers, 2015). Palaeosols indicate stagnation/displacement in the spring waters making up the travertines or pauses in tectonic activity (Chafetz and Folk, 1984; Guo and Riding, 1998; Özkul et al., 2002, 2010; Faccenna et al., 2008).

Climate. This study is the second to examine the travertine occurrences in Lake Van and surroundings (eastern Türkiye) in detail, and the first study in the Başkale Basin. In the first study, Yeşilova et al. (2021), have examined in detail their occurrence and development of the Edremit travertines and tufas. Edremit Travertine and Tufas are located ~85 km north-west of Dereiçi travertines. Therefore, this study will be correlated with the data of Yeşilova et al., (2021). Stages of travertine occurrence and palaeosol levels were used in comparing travertine occurrences with climate data. Palaeosols formed twice in the sequence, between 198.31 ±18 ka and 143.07 ±1.5 ka and between 96.73 ±8.34 ka and 61.59 ±5.4 ka. Lisiecki and Raymo (2005) examined the ^{18}O records of marine benthic stacks, with dating based on global glacial episodes. Stockhecke et al. (2014) studied the 600 ka sedimentary sequence of Lake Van, and indicated that the Lake Van deposits matched more than six glacial and interglacial periods of the marine record. When the formation times of the Dereiçi travertines are evaluated with their error bars and compared with the glacial and interglacial periods in the stratigraphy of Lisiecki and Raymo (2005), their occurrence coincides with the interglacial period in the second
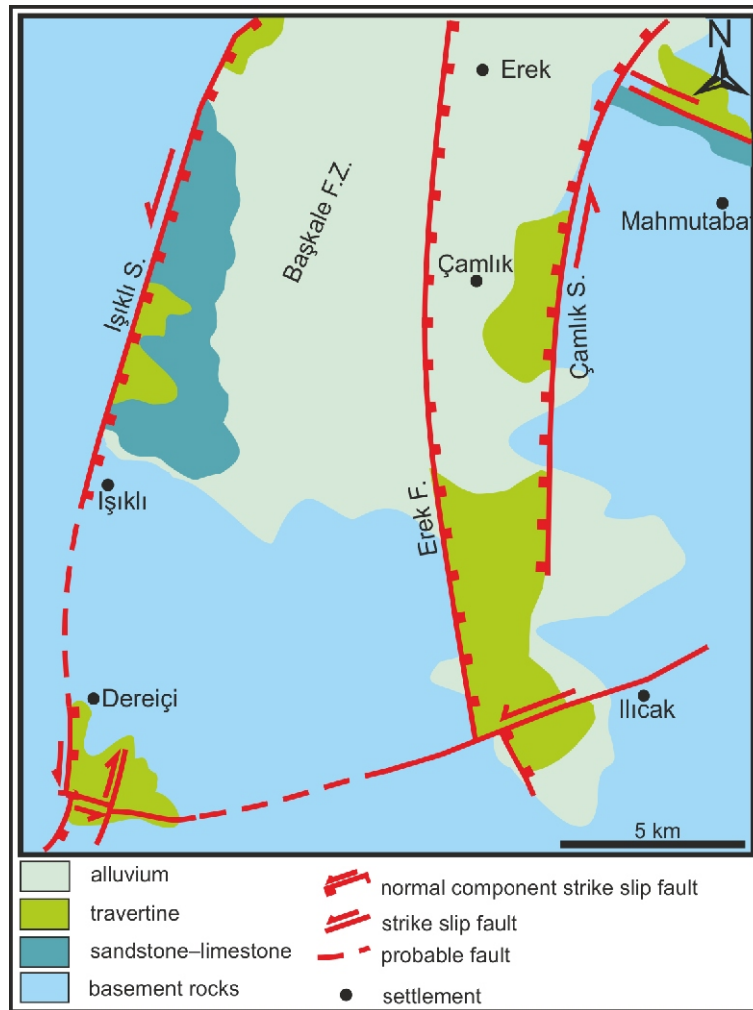
**Fig. 7. The fault systems forming the Başkale Fault Zone and the location
of the Dereiçi travertines on this fault system**

The figure is revised after Sağlam Selçuk and Düzgün (2017)

cycle (Fig. 6). The occurrence times of palaeosol lithofacies in the region coincide with glacial periods, though when the error bars in U/Th ages are taken into account, they also include interglacial periods (Fig. 6). Considering the error bars, one third of the interval of the 1st palaeosol (between 198.31 ±18–143.07 ±1.5 ka) corresponds to the interglacial period in the second cycle (Fig. 6). Again, when evaluated together with the error bars, it is seen that more than half of the 2nd palaeosol occurrence (between 96.73 ±8.34– 61.59 ±5.4 ka) coincides with the interglacial periods in the first cycle (Fig. 6). This situation suggests that palaeosols can form in both glacial and interglacial periods. The dates of travertine and palaeosol occurences with error bars are in accordance (Fig. 6) with the glacial and interglacial periods of the marine isotope stages (MIS) (NGRIP/GLT-syn ^{18}O; North Greenland Ice Core Project members 2004; Steffensen et al., 2008; Svensson et al., 2008; Wolff et al., 2010; Barker et al., 2011). Sporomorphs are also useful tools for interpreting past climate and vegetation. In Lake Van, detailed palynological and climatic studies were made by Litt et al. (2014). The travertine dates overlap with peaks of oak (*Quercus*) pollen from the interglacial periods (Fig. 6; e.g., Litt et al., 2014). Moreover, by correlating the Edremit travertine and tufas with the climate record, Yeşilova et al. (2019, 2021) suggested that these occurrences

were affected by climate, but not controlled by it. In the results obtained in this study, the occurrence times of both travertine and palaeosol are more compatible with climate influence (Fig. 6). The area where the travertines formed is 2250 m.a.s.l. During glacial periods, these areas would have been covered by thick glaciers (Akçar and Schlüchter, 2005). During glacial times, travertine occurrence will terminate because permafrost will prevent recharge of the aquifer (Yeşilova et al., 2019). However, travertine formation would continue anew in the temperate climate of interglacial periods (Yeşilova et al., 2019).

Tectonism. The Başkale Basin, a tectonically active area, is located on a plateau between the Arabian and Eurasian plates, resulting from collision that took place under a N–S trending compressional regime (Şengör and Kidd, 1979; Şengör and Yılmaz, 1981; Dewey et al., 1986; Şaroğlu and Yılmaz, 1986; Yılmaz et al., 1987; Koçyiğit et al., 2001; Utkucu et al., 2017; Gülyüz et al., 2019). There are many faults with potential to produce earthquakes in the Başkale Basin (Emre et al., 2012; Koçyiğit, 2013; Sağlam Selçuk and Düzgün, 2017). The faults forming the present morphology are the Işıklı, Ziraniş, Erek, Çamlık and Ilıcak faults, called the Batkale Fault Zone (Sağlam Selçuk and Düzgün, 2017; Fig. 7). The Dereiçi travertines are situated at the intersection of the Işıklı and the Ilıcak faults (Fig. 7).
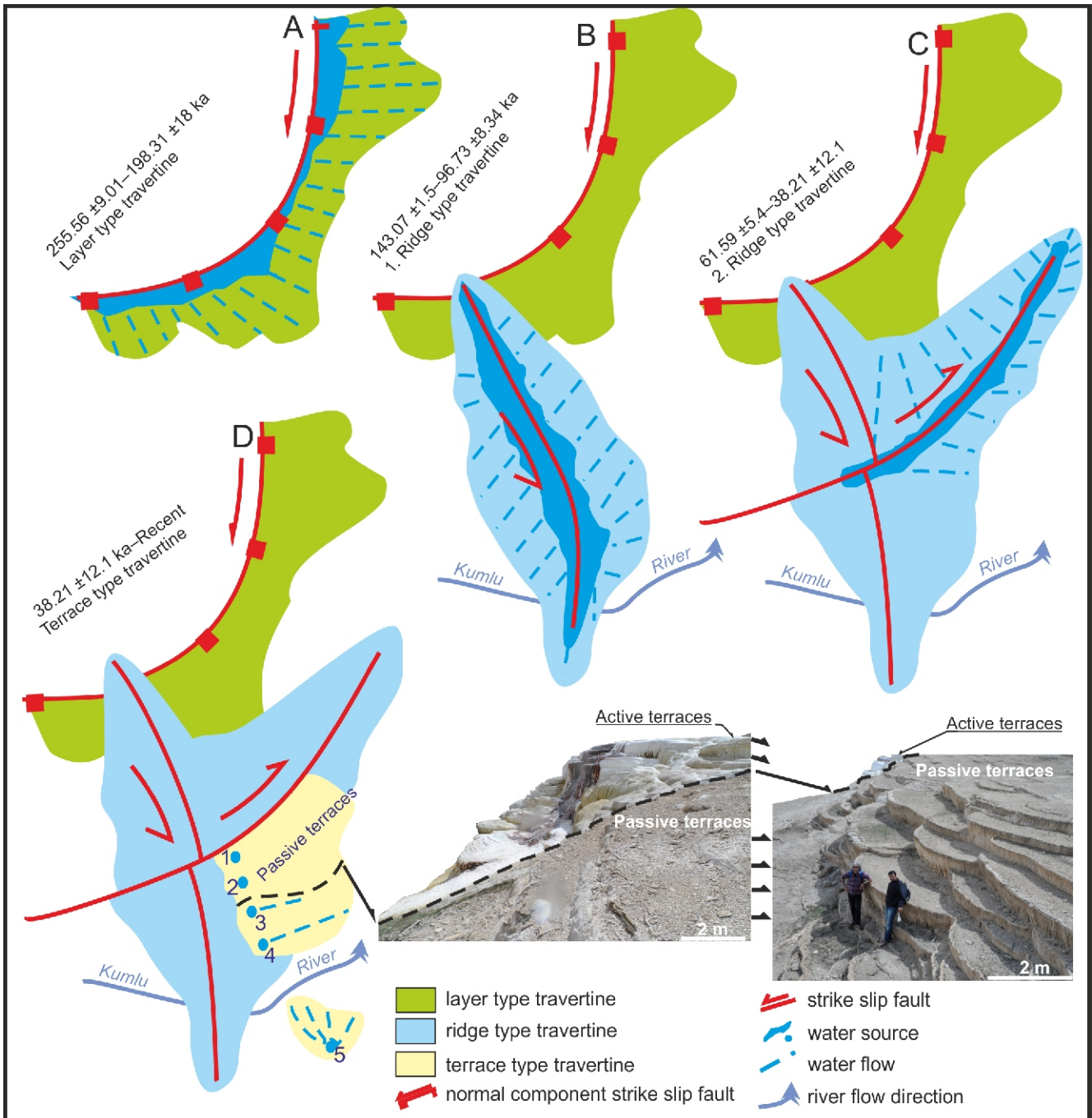
Fig. 8. Stages of travertine formation

The importance of fracture location, source location and flow direction of water in a travertine unit; **A** – layer type travertine; **B**, **C** – ridge type travertine; **D** – terrace type travertine (5 shows the newest, 1 the oldest water outlet); pictures showing the condition of active and passive terraces according to water outlets

The layer type travertines were formed along the fault plane from hydrothermal solutions carried by the Işıklı Fault to the surface (Fig. 8A). As the travertines formed between 255.56 ±9.01–198.31 ±18 ka, it would be appropriate to estimate an age of 255 ka or earlier for the age of the Işıklı Fault. In the time span of 57.25 ky between 255.56 ±9.01 ka and 198.31 ±18 ka, this fault was active. A palaeosol formed in the region as a result of erosion and weathering processes during the time interval of 198.31 ±18 to 143.07 ±1.5 ka (e.g., Kraus,

1999; Retallack, 2014; Tabor and Meyers, 2015). Between 143.07 ±1.5 and 96.73 ±8.34 ka, hydrothermal solutions emerging from the fracture, along the strike of the Ilıcak Fault, started to form the first ridge type travertine (Fig. 8B), at 46.34 ka. Therefore, the Ilıcak Fault was active around 46.34 ka. The Ilıcak Fault, which is ~143.07 ±1.5 ka or older, cut the older Işıklı Fault, and built younger travertines (Figs. 7 and 8). There is a phase without precipitation of travertines between 143.07 ±1.5 and 96.3 ka, represented by palaeosol oc-

Fig. 9. The Ilıcak Fault and related secondary faults, forming ridge type travertines (A, B); rising of thermal waters to the surface along fractures (C, D); collapses and fractures in travertines, and the study area (E, F).

currence due to pauses linked to tectonism or stagnation/displacement in the spring waters forming the travertines (e.g., Chafetz and Folk, 1984; Guo and Riding, 1998; Özkul et al., 2002, 2010; Faccenna et al., 2008). Sağlam Selçuk and Düzgün (2017) stated that the sub-basins bordered by the Işıklı and the Ziraniş faults (northern extension of Işıklı Fault) are younger than the other sub-basins and therefore these two faults control the Başkale Basin. They also pointed out that fault planes cut by secondary faults developed along the eastern slopes of the Işıklı and the Ziraniş faults (Fig. 7). The basin still migrates towards the east due to related faults. Another fault parallel to the Işıklı Fault formed a second ridge type travertine with secondary faults cutting the Işıklı Fault plane (Figs. 8C and 9A, B). Secondary faults also cut the Ilıcak Fault (Fig. 9A, B). Formation of the second ridge type travertine continued until 38.21 ±12.1 ka, after which the waters leaking from the fractures that opened along the slopes of the ridge type travertines produced the terrace type travertine (Fig. 8D). The terrace type
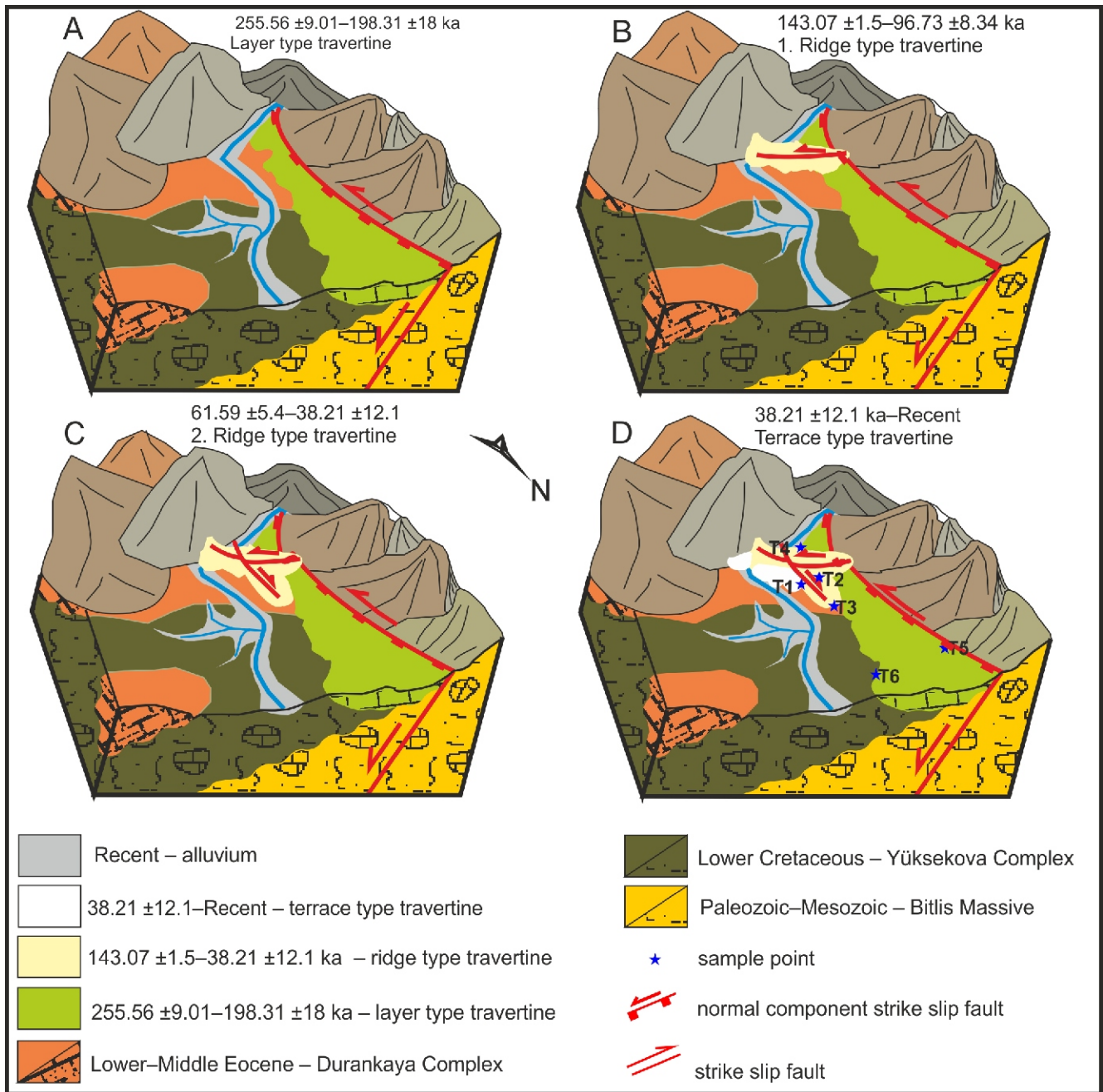
Fig. 10. Temporal representation of travertine development

travertine is the fourth and last travertine unit (see Fig. 2), and still continues to form (see Figs. 3G and 9A, B). The terrace type travertines young from NW to SE. While the first terraces are situated on the northwestern side of the travertines, other younger travertines are located on the southeastern side (see Figs. 3H and 8D).

Volcanism and magmatism. The oldest known volcanism in the Eastern Anatolian plateau commenced ~15 Ma (Lebedev et al., 2010) and continued until the year 1441 (Özdemir et al., 2006). The last oceanic lithosphere in the region was completely lost ~20 million years ago (Okay et al., 2010), and collision happened between 25 and 30 Ma (Oyan 2018a; Açlan and Altun 2018). The thin lithospheric mantle and the 38–45 km-thick crust (Zor et al., 2003; Angus et al., 2006; Özacar et al., 2008; Kind et al., 2015) led to the development of magmatic activity in the asthenospheric and lithospheric mantle (Keskin,

2003; Özdemir and Güleç, 2014; Oyan et al., 2016, 2017; Oyan, 2018b). Consequently, the hot mantle rose and melting continued throughout the Quaternary (Oyan et al., 2016, 2017; Oyan, 2018b). These events are the main reasons for the warming of groundwater and thermal activity (Yeşilova et al., 2021a). Moreover, CO_2 gas was released with volcanism at the end of glacial periods and led to carbonate dissolution in hydrothermal fluids (D'Alessandro et al., 2007; Huybers and Langmuir, 2009; Guido et al., 2010; Capezuoli et al., 2014). Hence, volcanism and magmatism in the region may be effective in warming the waters from which the travertines form. Geothermal gradients can also help warm these waters. Nevertheless, the influence of magmatism should be tested geochemically.

Water resources and geomorphology. The geomorphology and the source area are critical to the Dereiçi travertines
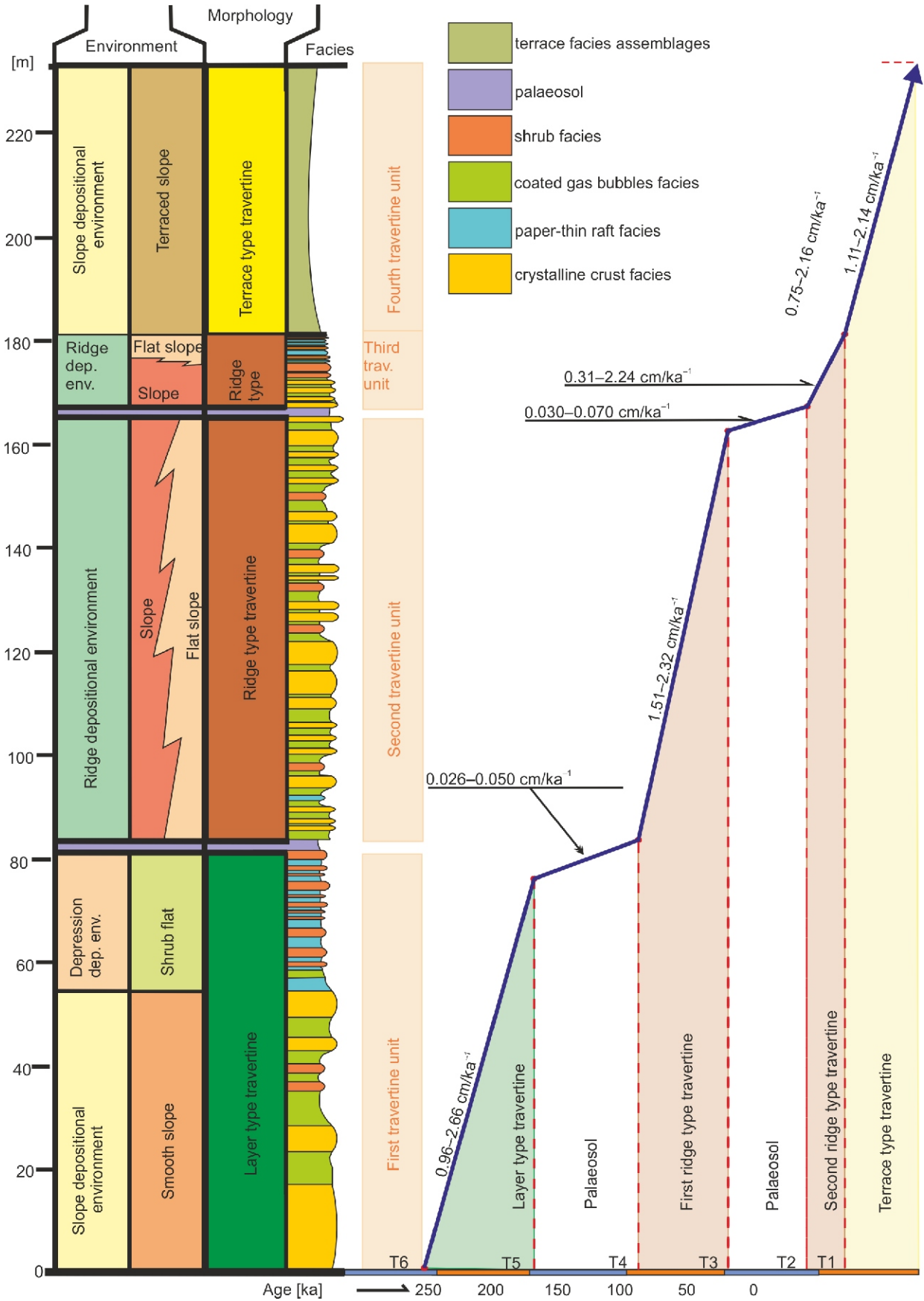
Fig. 11. Stages of growth of travertine around the Dereiçi area

(Chafetz and Folk, 1984; Pentecost, 1995; Guo and Riding, 1998; Özkul et al., 2002, 2010; Faccenna et al., 2008). Waters issuing from the fracture system, which developed perpendicular to the dip of the slope, flowed down the slope, and sourced the terrace type travertines (Figs. 8A and 10A). In the faults developed parallel to the dip of the slope, ridge type travertines were generated from water flowing from both sides of the fault (Figs. 8B, C and 10B, C). The terrace type travertine was formed by the hydrothermal waters flowing out at the intersection of two slopes with mutually perpendicular dips (Figs. 8D and 10D). During pauses at the source outlet, travertine formation ended and palaeosol developed (e.g., Chafetz and Folk, 1984; Guo and Riding, 1998; Özkul et al., 2002, 2010; Faccenna et al., 2008). The two palaeosol levels indicate the source outlet. The location of the recent post-palaeosol travertines indicates that the source exit points that controlled the travertines changed, as shown by the source change in terrace type travertines. These displacements in the source area are thought to result from tectonism and dense carbonate deposited from the spring water blocking the source outlet.

Growth stage of travertine. The growth rate of travertines is controlled by many factors such as climate, tectonism, water chemistry, geomorphology, vegetation, and biotic-abiotic mechanisms (Gradziński, 2010; Capezzuoli et al., 2014). The average growth speed of travertines has been determined as 20 cm/ka^{-1} (Pentecost, 2005). There are four different stages for development for the travertines in the area (Fig. 11). The first stage is the layer type travertine (Fig. 11), which formed in the time interval 255.56 ±9.01–198.31 ±18 ka, with a growth rate of 1.81cm/ka^{-1} (with the error bars, the lowest rate is 0.96 cm/ka^{-1}, and the highest is 2.66 cm/ka^{-1}). The second stage is the ridge type travertine (Fig. 11), which formed between 143.07 ±1.5 and 96.73 ±8.34 ka and had a growth rate of 1.915 cm/ka^{-1} (with error bars, 1,51 to 2.32 cm/ka^{-1}). The third stage is the ridge type travertine (Fig. 11), which formed between 61.59 ±5.4–38.21 ±12.1 ka and had a growth rate of 1.275 cm/ka^{-1} (error bars, the 0.31 to 2.24 cm/ka^{-1}). The fourth stage is the terrace type travertine with a growth rate of 1.625 cm/ka^{-1}, which formed from 38.21 ±12.1 ka to the present (Fig. 11; with error bars, 1.11 to 2.14 cm/ka^{-1}). The first ridge type travertine had the highest growth rate, whereas the second ridge type travertine had the lowest growth rate (Fig. 11). However, the average growth rate of almost all the travertines was 1 cm/ka^{-1} or more, though these values are far below the values suggested by previous studies (Pentecost, 2005). Possible reasons for the low values are: (i) open error bars, and (ii) the presence of palaeosols on the travertine successions showing erosion, and conditions at the source (water flow rate, calcium content). Considering that the largest of the three active springs currently forming travertines has a flow rate of 400 ml/s, the amount of water emerging from the spring is extremely low nowadays. However, the low amount of calcium in the source may also be a reason. Yeşilova et al. (2021) suggested that travertine growth velocities in the Edremit area (eastern Türkiye) were between 0.007 and 0.06 cm/ka^{-1}. The growth rates of the Dereiçi travertines are considerably higher than those of the Edremit travertines and tufas. There are long karst gaps in front of the slopes. As a result of these gaps, collapses occurred in the upper travertine deposits. The low growth velocities of travertine may therefore be linked to unidentified gaps (Fig. 10E, F; e.g., Gradziński et al., 2018).

The processes that affect the Dereiçi travertines are climate, tectonism, volcanism and magmatism. However, while the development of Dereiçi travertines is directly related to climate and tectonism, volcanism and magmatism are secondary processes as regards the Dereiçi travertines. The flow direction of the source and the geomorphology also shaped the morphology of the Dereiçi travertines.

CONCLUSIONS

Three factors were effective in forming the Dereiçi travertines. Climate and tectonism are the principal factors that controlled their development, while the geomorphology is responsible for their morphological diversity.

The times of deposition of the travertines reflected the fault history, the Işıklı Fault being active at 255.56 ±9.01 ka and earlier, and the Ilıcak Fault being active at 143.07 ±1.5 ka and earlier. However, the age of secondary faults developing on the fault slopes of the Işıklı Fault is 61.59 ±5.4 ka and earlier. Using this approach to constraining the timing of activity on the Işıklı Fault, which played an active role in developing the area, and the secondary faults developing on the fault plane, helps elucidate the tectonic evolution of the area.

REFERENCES

Açlan, M., Altun, Y., 2018. Syn-collisional I-type Esenköy Pluton (Eastern Anatolia – Turkey): an indication for collision between Arabian and Eurasian plates. Journal of African Earth Sciences, **142:** 1–11.

Akçar, N.C., Schlüchter., 2005. Paleoglaciations in Anatolia: a schematic review and first results. Eiszeitalter und Gegenwart, **55:** 102–121.

Altunel, E., Hancock, P.L., 1993a. Morphology and structural setting of Quaternary Travertines at Pamukkale, Turkey. Geological Journal, **28:** 335–346.

Altunel, E., Hancock, P.L., 1993b. Active fissuring faulting in Quaternary travertines at Pamukkale, western Turkey. Zeitschrift für Geomorphologie Supplement-Band, **94:** 285–302.

Andrews, J.E., 2006. Palaeoclimatic records from stable isotopes in riverine tufas: synthesis and review. Earth-Science Reviews, **75:** 85–104.

Angus, D.A., Wilson, D.C., Sandvol, E., Ni, J.F., 2006. Lithospheric structure of the Arabian and Eurasian collision zone in Eastern Turkey from S-wave receiver functions. Geophysical Journal of International, **166:** 1335–1346.

Barker, S., Knorr, G., Edwards, L., Parrenin, F., Putnam, A.E., Skinner, L.C., Wolff, E., Ziegler, M., 2011. 800,000 years of abrupt climate variability. Science, **334:** 347.

Barnes, L., Irwin, W.P., White, D.E., 1978. Global distribution of carbon dioxide discharges, and major zones of seismicity. U.S. Geological Survey, Water-Resources Investigations, Open-File Report, **78-39**.

Bertini, A., Minissale, A., Ricci, M., 2014. Palynological approach in upper Quaternary terrestrial carbonates of central Italy: anything but a "mission impossible". Sedimentology, **61**: 200–220.

Boray, A., 1975. Bitlis dolayının yapısı ve metamorfizması (in Turkish). Türkiye Jeoloji Bülteni, **18**: 81–84.

Brogi, A., Capezzuoli, E., 2009. Travertine deposition and faulting: the fault-related travertine fissure-ridge at Terme S. Giovanni, Rapolano Terme (Italy). International Journal of Earth Sciences, **98**: 931–947.

Brogi, A., Capezzuoli, E., 2014. Earthquake impact on fissure–ridge type travertine deposition. Geological Magazine, **151**: 1135–1143.

Brogi, A., Capezzuoli, E., Buracchi, E., Branca, M., 2012. Tectonic control on traver-tine and calcareous tufa deposition in a low-temperature geothermal system (Sarteano, Central Italy). Journal of the Geological Society, **169**: 461–476.

Brogi, A., Liotta, D., Ruggieri, G., Capezzuoli, E., Meccheri, M., Dini, A., 2016. An overview on the characteristics of geothermal carbonate reservoirs in southern Tuscany. Italian Journal of Geosciences, **135**: 17–29.

Capezzuoli, E., Gandin, A., Pedley, M., 2014. Decoding tufa and travertine (fresh water carbonates) in the sedimentary record: the state of the art. Sedimentology, **61**: 1–21.

Chafetz, H.S., Folk, R.L., 1984. Travertines: depositional morphology and the bacterially constructed constituents. Journal of Sedimentary Petrology, **54**: 289–316.

Chafetz, H.S., Rush, P.F., Utech, N.M., 1991. Microenvironmental controls on mineralogy and habit of $CaCO_3$ precipitates: an example from an active travertine system. Sedimentology, **38**: 107–126.

Cheng, H., Edwards, L.R., Shen, C.C., Polyak, V.J., Asmerom, Y., Woodhead, J., Hellstrom, J., Wang, Y., Kong, X., Spotl, C., Wang, X., Calvin, A.E., 2013. Improvements in ^{230}Th dating, ^{230}Th and ^{234}U half-life values, and U–Th isotopic measurements by multi-collector inductively coupled plasma mass spectrometry. Earth and Planetary Science Letters, **371**: 82–91.

Çukur, D., Krastel, S., Demirel-Schlüter, F., Demirbag, E., İmren, C., Niessen, F., Toker, M. and the PaleoVan-Working Group 2013. Sedimentary evolution of Lake Van (Eastern Turkey) reconstructed from high-resolution seismic investigations. International Journal of Earth Sciences, **102**: 571–585.

D'Alessandro, W., Giammanco, S., Bellomo, S., Parello, F., 2007. Geochemistry and mineralogy of travertine deposits of the SW flank of Mt. Etna (Italy): relationships with past volcanic and degassing activity. Journal of Volcanology and Geothermal Research, **165**: 64–70.

Dewey, J.F., Hempton, M.R., Kidd, W.S.F., Saroglu, F., Şengör, A.M.C., 1986. Shortening of continental lithosphere: The neotectonics of Eastern Anatolia – a young collision zone. Geological Society Special Publications, **19**: 1–36.

Dunham, R.J., 1962. Classification of carbonate rocks according to depositional texture. AAPG Memoir, **1**: 108–121.

Emre, Ö., Duman, T.Y., Özalp, S., Olgun, Ţ., Elmacı, H., 2012. 1:250,000 ölçekli Türkiye diri fay haritaları serisi, Van (NJ38-5) Paftası, Seri No 52 (in Turkish). Maden Tetkik ve Arama Genel Müdürlüğü, Ankara-Türkiye.

Faccenna, C., Soligo, M., Billi, A., De Filippis, L., Funiciello, R., Rossetti, C., Tuccimei, P., 2008. Late Pleistocene depositional cycles of the Lapis Tiburtinus travertine (Tivoli, Central Italy): possible influence of climate and fault activity. Global and Planetary Change, **63**: 299–308.

Folk, R.L., 1962. Spectral subdivision of limestone types. AAPG Memoir, **1**: 62–84.

Folk, R.L., Chafetz, H.S., Tiezzi, P.A., 1985. Bizarre forms of depositional and diagenetic calcite in hot-spring travertines, central Italy. SEPM Special Publication, **36**: 349–369.

Ford, T.D., Pedley, H.M., 1996. A review of tufa and travertine deposits of the world. Earth-Science Reviews, **41**: 117–175.

Fouke, B.W., Farmer, J.D., Des Marais, D.J., Pratt, L., Sturchio, N.C., Burns, P.C., Discipulo, M.K., 2000. Depositional facies and aqueous-solid geochemistry of travertine-depositing hot springs (Angel Terrace, Mammoth Hot Springs, Yellowstone National Park, U.S.A.). Journal of Sedimentary Research, **70**: 565–585.

Gandin, A., Capezzuoli, E., 2008. Travertine *versus* calcareous tufa: distinctive petrologic features and stable isotope signatures. Italian Journal of Quaternary Science, **21**: 125–136.

Gandin, A., Capezzuoli, E., 2014. Travertine: distinctive depositional fabrics of carbonates from thermal spring systems. Sedimentology, **61**: 264–290.

Gradziński, M., 2010. Factors controlling growth of modern tufa: results of a feld experiment. Geological Society Special Publications, **336**: 143–191.

Gradziński, M., Bella, P., Holúbek, P., 2018. Constructional caves in freshwater limestone: a review of their origin, classification, significance and global occurrence. Earth-Science Reviews, **185**: 179–201.

Griffiths, H.I., Pedley, H.M., 1995. Did changes in the late last glacial and early Holocene atmosphere CO_2 concentrations control the rates of tufa precipitation? Holocene, **52**: 238–242.

Guido, D.M., Channing, A., Campbell, K.A., Zamuner, A., 2010. Jurassic geothermal landscapes and fossil ecosystems at San Agustın, Patagonia, Argentina. Jounal of the Geological Society, **167**: 11–20.

Guido, D.M., Campbell, K.A., 2011. Jurassic hot spring deposits of the Deseado Massif (Patagonia, Argentina): characteristics and controls on regional distribution. Journal of Volcanology and Geothermal Research, **203**: 35–47.

Guo, L., 1993. Fabrics and facies of Quaternary travertines, Rapolano Terme, central Italy. Ph.D. thesis, Universty of Wales, Cardiff.

Guo, L., Riding, R., 1998. Hot-spring travertine facies and sequences, Late Pleistocene Rapolano Terme, Italy. Sedimentology, **45**: 163–180.

Göncüoğlu, M.C., Turhan, N., 1984. Geology of the Bitlis metamorphic belt. Maden Tetkik Arama yayınları, **1**: 237–244.

Göncüoğlu, M.C., Turhan, N., 1985. Bitlis Metamorfik kuţağı orta bölümünün temel jeolojisi (in Turkish). Mining Exploration Report No. 7707.

Gülyüz, E., Durak, H., Özkaptan, M., Krijgsman, W., 2019. Paleomagnetic constraints on the early Miocene closure of the southern Neo-Tethys (Van region; East Anatolia): inferences for the timing of Eurasia-Arabia collision. Global and Planetary Change, **185**, 103089.

Helvacı, C., Griffin, W.L., 1985. Rb-Sr geochronology of the Bitlis Massif, Avnik (Bingöl) area, S.E. Turkey. Special Publications of the Geological Societ, **17**: 403–413.

Huybers, P., Langmuir, C., 2009. Feedback between deglaciation, volcanism and atmospheric CO_2. Earth and Planetary Science Letters, **286**: 479–491.

Jones, B., 2017. Review of aragonite and calcite crystal morphogenesis in thermal spring systems. Sedimentary Geology, **354**: 9–23.

Julia, R., 1983. Travertines. AAPG Memoir, **33**: 64–72.

Kandemir, R., Tagliasacchi, E., Kayseri-Özer, M.S., Ţaffak, D., Köroğlu, F., Hsun-Ming H., Shen, C.C., 2021. The multidisciplinary approaches on facies developments and depositional systems of the Bahçecik Travertines, Gümüşhane, NE-Turkey. Turkish Journal of Earth Sciences, **30**: 561–579.

Keskin, M., 2003. Magma generation by slab steepening and breakoff beneath a subduction accretion complex: an alternative model for collision-related volcanism in Eastern Anatolia,Turkey. Geophysical Research Letters, **30**: 8046–8050.

Kind, R., Eken, T., Tilmann, F., Sodoudi, F., Taymaz, T., Bulut, F., Yuan, X., Can, B., Schneider, F., 2015. Thickness of the lithosphere beneath Turkey and surroundings from Sreceiver functions. Solid Earth, **6**: 971–984.

Kitano, Y., 1963. Geochemistry of calcareous deposits found in hot springs. Journal of Earth Science, Nagoya University, **11**: 68–100.]

Koçyiğit, A., 2013. New field and seismic data about the intraplate strike-slip deformation in Van region, east Anatolian plateau, E. Turkey. Journal of Asian Earth Science, **62**: 586–605.

Koçyiğit, A., Yılmaz, A., Adamia, S., Kuloshvili, S., 2001. Neotectonic of East Anatolian Plateau (Turkey) and Lesser Caucasus: Implication for transition from thrusting to strike-slip faulting. Geodinamica Acta, **14**: 177–195.

Kraus, M., 1999. Paleosols in clastic sedimentary rocks: their geologic applications. Earth-Science Reviews, **47**: 41–70.

Lebedev, V.A., Sharkov, E.V., Keskin, M., Oyan, V., 2010. Geochronology of the Late Cenozoic volcanism in the area of Van Lake (Turkey): an example of the developmental dynamics for magmatic processes. Doklady Earth Sciences, **433**: 1031–1037.

Lisiecki, L.E., Raymo, M.E. 2005. A Pliocene-Pleistocene stack of 57 globally distributed benthic ^{18}O records. Paleoceanography, 20, PA1003, Data archived at the World Data Center for Paleoclimatology, Boulder, Colorado, USA.

Litt, T., Pickarski, N., Heumann, G., 2014. A 600,000 year long continental pollen record from Lake Van, Eastern Anatolia (Turkey). Quaternary Science Reviews, **104**: 30–41.

Luo, L., Wen, H., Capezzuoli E., 2021. Travertine deposition and diagenesis in Ca-deficiency perched hot spring systems: a case from Shihuadong, Tengchong, China. Sedimentary Geology, **414**: 1–17.

Mesci, B.L., Gürsoy, H., Tatar, O., 2008. The evolution of travertine masses in the Sivas area (central Turkey) and their relationships to active tectonics. Turkish Journal of Earth Sciences, **17**: 219–240.

Muir-Wood, R., 1993. Neohydrotectonics. Zeitschrift für Geomorphologie Supplement-Band, **94**: 275–284.

Okay, A.I., Zattin, M., Cavazza, W., 2010. Apatite fission-track data for the Miocene Arabia-Eurasia collision. Geology, **38**: 35–38.

Ordonez, S., Gonzalez, J.A., Garcia del Cura, M.A., 1986. Pétrographie et morphologie des édifices tuffeux quaternaires du centre de l'Espagne. Méditerranée, **57**: 52–60.

Oyan, V., 2018a. Ar\Ar dating and petrogenesis of the Early Miocene Taţkapı-Mecitli (Erciş-Van) granitoid, Eastern Anatolia Collisional Zone, Turkey. Journal of Asian Earth Sciences, **158**: 210–226.

Oyan, V., 2018b. Geochemical and petrologic evolution of Otlakbaţı basaltic volcanism to the east of Lake Van. Bulletin of the Mineral Research and Exploration. **157**: 1–21.

Oyan, V., Keskin, M., Lebedev, V.A., Chugaev, A.V., Sharkov, E.V., 2016. Magmatic evolution of the Early Pliocene Etrüsk stratovolcano, Eastern Anatolian Collision Zone, Turkey. Lithos, **256–257**: 88–108.

Oyan, V., Keskin, M., Lebedev, V.A., Chugaev, A.V., Sharkov, E.V., Ünal, E., 2017. Petrology and geochemistry of the Quaternary mafic volcanism in the north-east of Lake Van, Eastern Anatolian Collision Zone, Turkey. Journal of Petrology, **58**: 1701–1728.

Özacar, A.A., Gilbert, H., Zandt, G., 2008. Upper mantle discontinuity structure beneath East Anatolian Plateau (Turkey) from receiver functions. Earth and Planetary Science Letters, **269**: 426–434.

Özdemir, Y., Güleç, N., 2014. Geological and geochemical evoluation of Suphan stratovolcano Eastern Anatolia, Turkey: evidence for the lithosphere-asthenosphere interaction on post collisional volcanism. Journal of Petrology, **55**: 37–62.

Özdemir, Y., Karaoğlu, Ö., Tolluođlu, A.Ü., Güleç, N., 2006. Volcanostratigraphy and petrogenesis of the Nemrut stratovolcano (East Anatolian High Plateau): the most recent postcollisional volcanism in Turkey. Chemical Geology, **226**: 189–211.

Özkul, M., Alçiçek, M.C., Heybeli, H., Semiz, B., Erten, H., 2001, Depositional features of Denizli hot spring travertines and their appraisement in view marbling (in Turkish with English summary). III Turkey Marble Symposium (Mersem'2001) Proceeding Book: 57–72, Afyon, Turkey.

Özkul, M., Varol, B., Alçiçek, M.C., 2002. Depositional environments and petrography of the Denizli travertines. Bulletin of Mineral Research Exploring, **125**: 13–29.

Özkul, M., Gökgöz, A., Horvatinčić, N., 2010. Depositional properties and geochemistry of Holocene perched springline tufa deposits and associated spring waters: a case study from the Denizli province, Western Turkey. Geological Society Special Publications, **336**: 245–262.

Özkul, M., Gökgöz, A., Sandor, K., Baykara, M.O., Shen, C.C., Chang, Y.W., Kaya, A., Hançer, M., Aratman, C., Taylan, A., Örü, Z., 2014. Sedimentological and geochemical characteristics of a fluvial travertine: a case from the eastern Mediterranean region. Sedimentology, **61**: 291–318.

Pedley, H.M., 1990. Classification and environmental models of cool freshwater tufas. Sedimentary Geology, **68**: 143–154.

Pentecost, A., 1995. The Quaternary travertine deposits of Europe and Asia Minor. Quaternary Science Reviews, **14**: 1005–1028.

Pentecost, A., 2005. Travertine. Springer, Berlin.

Perinçek, D., 1979. The Geology of Hazro-Korudağ-Çüngüẗ-Maden-Ergani-Elazığ-Malatya area. Guide Book, Türkiye Jeoloji Kurumu yayını, **1**: 33– 47.

Perinçek, D., 1990. Hakkâri ili ve dolayının stratigrafisi, GDA Türkiye (in Turkish). TPJD Bülteni, **2**: 21–68.

Piper, J.D., Mesci, L.B., Gürsoy, H., Tatar, O. and Davies, C.J., 2007. Palaeomagnetic and rock magnetic properties of travertine: its potential as a recorder of geomagnetic palaeosecular variation, environmental change and earthquake activity in the Sıcak Cermik geothermal field, Turkey. Physics of the Earth and Planetary Interiors, **161**: 50–73.

Retallack, G.J., 2014. Paleosols and paleoenvironments of early Mars. Geology **42**: 755–758.

Richmond, G.M., 1962. Quaternary stratigraphy of the La Sal Mountains, Utah. U.S. Geological Survey Professional Paper, **324**.

Ricou, L., 1971. Le croissant ophiolitique péri-arabe: une ceinture de nappes mises en place au Crétacé supérieur. Revue de Geologie Dynamique et de Geographie Physique, **13**: 327–350

Sağlam Selçuk, A., 2016. Evaluation of the relative tectonic activity in the eastern Lake Van basin, East Turkey. Geomorphology, **270**: 9–21.

Sağlam Selçuk, A., Düzgün, M., 2017. Tectonic geomorphology of başkale fault zone. Bulletin of the Mineral Research and Exploration, **155**: 33–46.

Shen, C.-C., Cheng, H., Edwards, R.L., Moran, S.B., Edmonds, H.N., Hoff, J.A., Thomas, R.B., 2003. Measurement of attogram quantities of ^{231}Pa in dissolved and particulate fractions of seawater by isotope dilution thermal ionization mass spectroscopy. Analytical Chemistry, **75**: 1075–1079.

Shen, C.-C., Wu, C.-C., Cheng, H., Edwards, R.L., Hsieh, Y.-T., Gallet, S., Chang, C.-C., Li, T.-Y., Lam, D.D., Kano, A., Hori, M., Spötl, C., 2012. High-precision and high-resolution carbonate ^{230}Th dating by MC-ICP-MS with SEM protocols. Geochimica et Cosmochimica Acta, **99**: 71–86.

Sibson, R.H., Moore, J.M.M., Rankin, A.H., 1975. Seismic pumping a hydrothermal fluid trans port mechanism. Journal of the Geological Society, **131**: 653–659.

Steffensen, J.P., Andersen, K.K., Bigler, M., Clausen, H.B., Dahl-Jensen, D., Fischer, H., Goto-Azuma, K., Hansson, M., Johnsen, S.J., Jouzel, J., Masson-Delmotte, V., Popp, T., Rasmussen, S.O., Röthlisberger, R., Ruth, U., Stauffer, B., Siggaard-Andersen, M.L., Sveinbjörnsdóttir, A.E., Svensson, A.,White, J.W.C., 2008. High–resolution Greenland ice core data show abrupt climate change happens in few years. Science, **321**: 680–684.

Stockhecke, M., Sturm, M., Brunner, I., Schmincke, H.U., Sumita, M., Kipfer, R., Çukur, D., Kwiecien, Anselmetti, F.S., 2014. Sedimentary evolution and environmental history of Lake Van (Turkey) over the past 600,000 years. Sedimentology, **61**: 1830–1861.

Svensson, A., Andersen, K.K., Bigler, M., Clausen, H.B., Dahl-Jensen, D., Davies, S.M., Johnsen, S.J., Muscheler, R., Parrenin, F., Rasmussen, S.O., Röthlisberger, R., Seierstad, I., Steffensen, J.P., Vinther, B.M., 2008. A 60 000 year Greenland stratigraphic ice core chronology. Climate of the Past, **4**: 47–57.

Şaroğlu, F., Yılmaz, Y., 1986. Doğu Anadolu'da neotektonik donemdeki jeolojik evrim ve havza modelleri. Mineral Research Exploring Instute (MTA) Bulletin, **107**: 73–94.

Şengör, A.M.C., Kidd, W.S.F., 1979. Post-collisional tectonics of the Turkish-Iranian plateau and a comparison with Tibet. Tectonophysics, **55**: 361–376.

Şengör, A.M.C., Yılmaz, Y., 1981. Tethyan evolution of Turkey: a plate tectonic approach. Tectonophysics, **75**: 181–190..

Şengün, M., 1984. Tatvan güneyinin (Bitlis masifi) jeolojik/petrografik incelenmesi (in Turkish). Ph.D. thesis, University of Hacettepe, Ankara, Türkiye.

Tabor, N.J., Myers, T.S., 2015. Paleosols as indicators of paleoenvironment and paleoclimate. Annual Reviews Earth Science, **43**: 333–361.

Tagliasacchi-Toker, E., 2018. Orta-geç Pleistosen Gürlek-Kocabaş (Denizli) ve Örtülü (Afyon) travertenlerinin paleoçevresel gelişimi, SW. Türkiye (in Turkish). Türkiye Jeoloji Bülteni, **60**: 1–22.

Tagliasacchi-Toker, E., Kayseri-Özer, M.S., 2020. Multidisciplinary approach signals of the non-marine carbonates: The case of the Sarıkavak tufa deposits (Afyon, SW-Turkey). Quaternary International, **544**: 41–56.

Toker, E., 2017. Quaternary fluvial tufas of Sarıkavak area, southwestern Turkey: facies and depositional systems. Quaternary International, **437**: 37–50.

Toker, E., Kayseri-Özer, M.S., Özkul, M., Kele, S., 2015. Depositional system and palaeoclimatic interpretations of middle to late Pleistocene travertines: Kocabaş, Denizli, SW Turkey. Sedimentology, **62**: 1360–1383.

Toker, M., 2013. Time-dependent analysis of aftershock events and structural impacts on intraplate crustal seismicity of the Van earthquake (Mw 7.1, 23 October 2011), E-Anatolia. Central European Journal of Geosciences, **5**: 423–434.

Toker, M., 2014. Discrete characteristics of the aftershock sequence of the 2011 Van earthquake. Journal of Asian Earth Science, **92**: 168–186.

Toker, M., Şahin, S., 2019. Crustal Poisson's ratio tomography and velocity modeling across tectono-magmatic lake regions of Eastern Anatolia (Turkey): new geophysical constraints for crustal tectonics. Journal Geodynamica, **131**: 1–28.

Toker, M., Tur, H., 2018. Structural patterns of the Lake Erçek Basin, eastern Anatolia (Turkey): evidence from single-channel seismic interpretation. Marine Geophysical Research, **39**: 567–588.

Toker, M., Şengör, A.M.C., Demirel-Schluter, F., Demirbağ, E., Çukur, D., Imren, C., Niessen, F., Group P.-W., 2017a. The structural elements and tectonics of the Lake Van basin (Eastern Anatolia) from multi-channel seismic reflection profiles. Journal of African Earth Sciences, **129**: 165–178.

Toker, M., Pınar, A., Tur, H., 2017b. Source mechanisms and faulting analysis of the aftershocks in the Lake Erçek area (Eastern Anatolia, Turkey) during the 2011 Van event (Mw 7.1): implications for the regional stress field and ongoing deformation processes. Journal of Asian Earth Science, **150**: 73–86.

Tolluoğlu, A.Ü., 1981. Mutki (Bitlis) yöresi metamorfiklerinin petrografisi/petrolojisi (in Turkish). Yüksek Mühendislik Tezi, Hacettepe Üniversitesi, Ankara.

Utkucu, M., Kızılbuğa, S., Arman, H., 2017. Constraining fault rupture of the 27 November 2005 Qeshm Island (Iran) earthquake (M_W=6.0) in the Arabian gulf from the inversion of the teleseismic broadband waveforms. Extended abstract, fourth international conference on engineering geophysics, proceedings book, October 9–12, 2017 United Arab Emirates University, Al Ain.

Van Noten, K., Topal, S., Baykara, O., Özkul, M., Claes, H., Aratman, C., Swennen, R., 2018. Pleistocene-Holocene tectonic reconstruction of the Ballık travertine (Denizli Graben, SW Turkey): (de)formation of large travertine geobodies at intersecting grabens. Journal of Structural Geology, **118**: 114–134.

Veysey, J., Fouke, B.W., Kandianis, M.T., Schickel, T.J., Johnson, R.W., Goldenfeld, N., 2008. Reconstruction of water temperature, pH, and flux of ancient hot springs from travertine depositional facies. Journal of Sedimentary Research, **78**: 69–76.

Wolff, E.W., Chappellaz, J., Blunier, T., Rasmussen, S.O., Svensson, A., 2010. Millennial-scale variability during the last Glacial: the ice core record. Quaternary Science Reviews, **29**: 2828–2838.

Yeşilova, Ç., 2021. Potential geoheritage assessment: Dereiçi Travertines, Başkale, Van (east anatolian Turkey). Manas Journal of Engineering. **9**: 66–71.

Yeşilova, ç., Gülyüz E., Ci-Rong H., Chuan-Chou S., 2019. Giant tufas of Lake Van record lake-level fluctuations and climatic changes in eastern Anatolia, Turkey. Palaeogeography Palaeoclimatology Palaeoecology, **533**: 1–9.

Yeşilova, Ç., Güngör-Yeşilova, P., Açlan, M., Tsai-Luen, Y., Chuan-Chou, S., 2021. U-Th ages and facies properties of Edremit travertine/tufas, Van, Eastern Anatolia: implications of Neo-tectonic for the region. Geological Quarterly, **65**: 28.

Yılmaz, O., 1975. Cacas bölgesi (Bitlis Masifi) kayaçlarının petrografik ve stratigrafik incelenmesi (in Turkish). Türkiye Jeoloji Kurumu Bülteni, **18**: 33–41.

Yılmaz, Y., 1971. Etüde petrographicque et geochronologique de la region de Casa (Partie Meridionale du Masif de Bitlis, Turquie, These de doct 3 cycle). Univ. Sci.Med. Greonable.

Yılmaz, Y., Şaroglu, F., Güner, Y., 1987. Initiation of the neomagmatism in East Anatolia. Tectonophysics, **134**: 177–199.

Zor, E., Gürbüz, C., Türkelli, N., Sandvol, E., Seber, D., Barazangi, M., 2003. The crustal structure of the East Anatolian Plateau from receiver functions. Geophysical Research Letters, **30**: 8044–8047.